POLITECNICO DI TORINO
Repository ISTITUZIONALE

Benchmark on the Aerodynamics of a Rectangular 5:1 Cylinder: An overview after the first four years of activity

*Original*
Benchmark on the Aerodynamics of a Rectangular 5:1 Cylinder: An overview after the first four years of activity / Bruno, Luca; Maria Vittoria, Salvetti; Francesco, Ricciardelli. - In: JOURNAL OF WIND ENGINEERING AND INDUSTRIAL AERODYNAMICS. - ISSN 0167-6105. - STAMPA. - 126:(2014), pp. 87-106. [10.1016/j.jweia.2014.01.005]

*Availability:*
This version is available at: 11583/2537908 since:

*Publisher:*
Elsevier

*Published*
DOI:10.1016/j.jweia.2014.01.005

*Terms of use:*

This article is made available under terms and conditions as specified in the corresponding bibliographic description in the repository

*Publisher copyright*

(Article begins on next page)

19 April 2024

# Benchmark on the Aerodynamics of a Rectangular 5:1 Cylinder: an overview after the first four years of activity

Luca Bruno [a,*] Maria Vittoria Salvetti [b], Francesco Ricciardelli [c]

[a] *Politecnico di Torino, DAD*
*Viale Mattioli 39, I-10125, Torino, Italy*

[b] *University of Pisa, DICI*
*Via Girolamo Caruso 8, I-56122, Pisa, Italy*

[c] *University of Reggio Calabria, DIIIES*
*Via Graziella, Feo di Vito, I-89122, Reggio Calabria, Italy*

**Abstract**

In July 2008, a benchmark study on the aerodynamics of a stationary rectangular cylinder with chord-to-depth ratio equal to 5 (BARC) was launched. This paper gives an outline of the state of the art on the aerodynamics of 5:1 rectangular cylinders prior to the starting of BARC, and summarizes the results obtained by the contributors during the first four years of activity. The results of about 70 realisations of the BARC flow configuration obtained under nominally common setup in both wind tunnel experiments and numerical simulations are compared mutually and with the data available in the literature prior to BARC, in terms of bulk parameters, flow and aerodynamic load statistics, pressure and force spanwise correlations. It is shown that the near wake flow, the base pressure and, hence, the drag coefficient obtained in the different flow realisations are in very good agreement. Conversely, the flow features along the cylinder lateral surfaces and, hence, the lift are strongly sensitive to setup and modelling, leading to a significant dispersion of both wind tunnel measurements and numerical predictions. Finally, a possible asymmetry of the time averaged flow has been recognised both in wind tunnel tests and in numerical simulations.

*Key words:* Bluff-body aerodynamics, BARC benchmark, numerical simulations, wind tunnel tests

* Corresponding author. Tel: (+39) 011.090.4870. Fax: (+39) 011.090.4999.
*Email address:* luca.bruno@polito.it (Luca Bruno).

## 1 Introduction

In July 2008, a benchmark study on the aerodynamics of rectangular cylinders (a Benchmark on the Aerodynamics of a Rectangular 5:1 Cylinder, BARC) was announced during the VI Colloquium on Bluff Body Aerodynamics and Applications (BBAA VI). This paper aims at providing a progress report of the BARC activities four years after its announcement.
BARC is aimed at establishing a platform for discussion among scientists working on bluff body aerodynamics, and in particular it concerns the analysis of the turbulent, separated flow around an elongated rectangular cylinder. The characteristics of the flow field around rectangular bodies is of great interest both for fundamental research and for applications. From the fundamental research point of view, in spite of the simple and nominally two-dimensional geometry, the flow over an elongated rectangular cylinder at high Reynolds numbers is highly complex, being three dimensional, turbulent and characterized by unsteady flow separation and reattachment. The main flow features of the BARC configuration are described in more detail in the following. On the other hand, thanks to the simple geometry, a detailed analysis of the flow dynamics can be carried out, and different patterns, which can also be found when dealing with more complex geometries, can be identified. As for applications, this benchmark problem provides useful information on the aerodynamics of a wide range of bluff bodies of interest in civil engineering (e.g. long-span bridge decks or high-rise buildings) as well as in other engineering areas.
It is well known that rectangular cylinders are characterized by one single geometric parameter, i.e. the ratio of the alongwind dimension (Breadth) to the crosswind dimension (Depth), $B/D$, which governs their aerodynamic behaviour (see e.g. [Nakaguchi et al., 1968, Stokes and Welsh, 1986]). Other geometric (e.g. surface roughness, corner sharpness) and flow parameters (e.g. Reynolds number, turbulence intensity and scale) play a major or minor role, depending on the $B/D$ value and on their range of variability. For small $B/D$ ratios ($< 2.5$), the flow separates from the leading edge and does nor reattach to the side faces of the cylinder, with vortex shedding occurring only from the leading edge. For larger $B/D$ ratios, the shear layer impinges on the side faces of the cylinder. For moderate $B/D$ ratios (roughly between 2.5 and 3.5), reattachment is intermittent, and vortex shedding still occurs only from the leading edge. For $B/D$ ratios greater than 3.5, reattachment is permanent, and vortex shedding occurs from both the leading and the trailing edges. Under this circumstance, the flow patterns depends on $B/D$ in a discontinuous fashion. Trailing edge shedding is influenced by the dynamics of the shear layer detaching at the usptream corners and impinging on the side face downstream of the separation bubble; the breadth-based Strouhal number is a multiple of $0.55 \div 0.60$, depending on the number of vortices simultaneously attached to each face of the cylinder (see e.g. [Nakamura et al., 1991, Stokes and Welsh,

1986]). For $B/D < 6$ the Strouhal number is $1 \times (0.55 \div 0.60)$, for $6 < B/D < 9$ the Strouhal number is $2 \times (0.55 \div 0.60)$, for $9 < B/D < 12$ it is $3 \times (0.55 \div 0.60)$. It follows that the choice made for the BARC of a $B/D$ ratio of 5 aims at having a completely reattached flow ($B/D > 3.5$) and simultaneously one single attached vortex on each face of the cylinder ($B/D < 6$).
In the following the studies published prior to the BARC announcement are briefly reviewed, in order to provide the context in which the BARC benchmark was launched. The overview is limited to the aerodynamics of rectangular cylinders with $B/D$ ratio equal to 5 or close to it, i.e. $3.5 \leq B/D \leq 6$. Bearing in mind that BARC addresses both the wind tunnel and the computational approaches, they are discussed separately.
The reviewed wind/water tunnel studies are chronologically listed in Table 1. For the sake of clarity, the listed references can be grouped in two subsets

Table 1
Wind/water tunnel studies around rectangular cylinders prior to BARC

| Authors | $B/D$ | $\mathrm{Re}_D$ | $L/D$ | Blockage (%) | $I_u$ (%) |
|---|---|---|---|---|---|
| Nakamura and Yoshimura [1982] | 0.2-5 | 5500-140000 | 10;25 | 2;5 | 0.1 |
| Okajima [1982] | 1-4 | 200-20000 | 13.3-100 | $< 2.5$ | $< 0.5\%$ |
| Okajima et al. [1983] | 1-9 | 42000 | – | 1 | 0.4 |
| Parker and Welsh [1983] | $< 52$ | 15000-31000 | 203 | 0.25 | 0.2 |
| Stokes and Welsh [1986] | $< 16$ | 8000-44300 | 203-407 | 0.25-0.49 | 0.2 |
| Nakamura and Nakshima [1986] | 1-10 | 2500-300000 | 3-30 | $\leq 6$ | – |
| Nakamura et al. [1991] | 3-16 | 1000-3000 | 100 | 0.17 | 0.3 |
| Matsumoto et al. [2003] | 5 | — | 15 | 3 | – |
| Ricciardelli and Marra [2008] | 5 | 63600 | 38.7 | 3.5 | $\simeq 1$ |
| Le et al. [2009] | 1;5 | 18000-54000 | 10.4 | – | 9.5-11.5 |
| Ricciardelli [2010] | 5 | 64000 | 38.7 | 3.5 | $\simeq 1$ |

by referring to both the chronological and thematic criteria. The studies developed in the eighties and nineties mainly investigate the variability of the aerodynamic behaviour versus the $B/D$ ratio by means of force and/or velocity measurements. The more recent works focus their attention on the ratio $B/D = 5$ and on the spanwise coherence of the flow by means of pressure measurements over the cylinder surface. From the results of wind and water tunnel experiments on rectangular prisms with $B/D = 1$, 2, 3 and 4, at Reynolds numbers in the range of 70 to 20,000, Okajima [1982] investigated the variation of the Strouhal number and flow characteristics with the Reynolds number. He concluded that the minimum aspect ratio giving rise to flow reattachment is Reynolds number dependent, and tends to 2.8 at high Reynolds number. Conversely, the minimum Reynolds number giving rise to fully separated flow depends on the aspect ratio. In Okajima et al. [1983] the variation of the drag and lift coefficients and of the Strouhal number with the aspect ratio was investigated, and the existence of an unsteady reattachment of the separated shear layer on the side surfaces for values of the aspect ratio in the range of 2.0 to 2.8 was pointed out. Parker and Welsh [1983] and Stokes and Welsh [1986]

analysed the effects that the application of sound has on the characteristics of the shear layer and of the separation bubble of rectangular cylinders with $B/D$ ratios up to 52. Nakamura and Nakshima [1986] suggested that for rectangular cylinders with $B/D$ in the range 3-15 the vortex shedding mechanism is not of Karman type, i.e. triggered directly by the interaction between upper and lower shear layers, but it is due to the impinging shear layer instability. They also showed that shear layer instability, vortex shedding and vortex excitation were possible also in the presence of a splitter plate, and observed that vortex excitation was possible for elastically suspended models for which hot-wire measurements had not shown sharp spectra at rest. Successively, in Nakamura et al. [1991] the characteristics of vortex shedding from rectangular cylinders with $3 < B/D < 13$ was investigated, and the discontinuous variation of the Strouhal number earlier pointed out was found.
In Matsumoto et al. [2003] the spanwise coherence of pressure fluctuations on a rectangular cylinder with $B/D = 5$ was investigated through wind tunnel tests in smooth and turbulent flow. The tests confirmed the largest coherence of pressure fluctuations with respect to those of the incoming flow. Ricciardelli and Marra [2008] discussed the sectional distribution of the statistics (mean, standard deviation, skewness and kurtosis) of the pressure coefficients on a rectangular stationary and vibrating cylinder with $B/D = 5$, as derived from wind tunnel experiments. In addition the spanwise correlation of pressure fluctuations was also discussed, in the cases of smooth and turbulent incoming flow. In Ricciardelli [2010], the effects of the vibration regime on the spanwise correlation of aerodynamic forces and of stagnation and base pressure for a rectangular cylinder with $B/D$ =5 were discussed, as derived from wind tunnel tests. Le et al. [2009] analysed the results obtained by means of wind tunnel tests for a highly turbulent incoming flow ($10\% \leq I_x \leq 12\%$) around a square and a rectangular 5:1 cylinder. First, statistics on chordwise pressure distribution were discussed. Second, Fourier and wavelet spectra of spanwise coherent turbulent structures and of pressure were analysed. The differences from the case of the fully separated and reattached flow were pointed out, and the larger coherence of pressures with respect to turbulent fluctuations was confirmed.
Computational studies on the aerodynamics of rectangular cylinders available prior to the announcement of BARC are chronologically listed in Table 2. Both two-dimensional(2D) and three-dimensional (3D) features of the low-Reynolds number flow ($10^2 \leq Re \leq 10^3$) around rectangular cylinders have been clarified in several studies, e.g. Nakamura et al. [1996], Ohya et al. [1992], Hourigan et al. [2001], Tan et al. [2004]. However, being this flow conditions rather away from those of interest for BARC, these studies are not reviewed herein, and interested readers can refer to the cited papers and to their references. On the other hand, the high-Reynolds number flow conditions (i.e. Re$\geq 10^4$) have been investigated using computational techniques with special emphasis on the dependence of the aerodynamic behaviour on the chord-to-depth ratio, e.g. in Shimada and Ishihara [2002], Tamura and Ito

Table 2
Computational studies around rectangular elongated cylinders previous to BARC

| Authors | turb. mod. | $B/D$ | $\mathrm{Re}_D$ | $L/D$ |
|---|---|---|---|---|
| Tamura et al. [1993] | no model | 5 | $10^4$ | 2 |
| Tamura and Ito [1996] | no model | $0.6 \leq B/D \leq 8$ | $10^4$ | 2 |
| Yu and Kareem [1998] | LES | $1 \leq B/D \leq 4$ | $10^5$ | 2 |
| Shimada and Ishihara [2002] | RANS | $0.6 \leq B/D \leq 8$ | $2. \times 10^4$ | 0 (2D) |

[1996], Yu and Kareem [1998]. In particular, Shimada and Ishihara [2002] also investigated, among others, the rectangular 5:1 cylinder in a 2D domain with a two-layer modified $k\varepsilon$ RANS turbulence model. Their computations succeeded in reproducing a smooth and periodic vortex shedding also at high Reynolds numbers, as well as the discontinuity in the Strouhal number at $B/D = 2.8$ and $B/D = 6.0$. Nonetheless, the pressure and force fluctuations were underestimated. The authors argued that this is due to Reynolds averaging of the Navier-Stokes equations. Tamura and Ito [1996] discretized the 3D NavierStokes equations through a finite-difference technique at $Re = 10^4$ and studied the mechanism of vortex formation for several rectangular cylinders with different $B/D$ ratios. To our knowledge, only Tamura et al. [1993] focused on the rectangular 5:1 cylinder by using a finite-difference discretisation of the NavierStokes equations on structured O-grids in 2D and 3D. A third-order upwind scheme was adopted for the convective terms and no turbulence model was employed. The separation bubble was recognized to be responsible of irregularly fluctuating pressure patterns around the reattachment area on the side surface. The dynamic characteristics of the shear layer separated from the leading edge and the instability of the strong shear region to form the wake vortices were discussed by comparing two- and three-dimensional computed flows. In a successive work [Tamura et al., 1995] also the forced oscillating cylinder was studied at the same incoming flow conditions by means of a 2D model.
In this context, the aims of BARC have been specified to be following [Bartoli et al., 2008a]:

- to deeply investigate one specific problem in bluff-body aerodynamics, with contributions coming from as many researchers as possible worldwide;
- to assess the consistency of wind tunnel measurements carried out in different facilities;
- to assess the consistency of computational results obtained through different flow models and numerical approaches;
- to compare wind tunnel measurements and computational results;
- to assess the possibility of developing integrated procedures relying on both wind tunnel and computational outcomes;
- to develop Best Practice Advice for wind tunnel tests and computational

simulations;
- to organize and to make available to the scientific and technical communities a database of the results provided by the participants for future reference.

Note that the BARC has not adopted a single set of measurements as a reference at its launching. This choice is driven by the fact that: (i) both wind tunnel tests and computational simulations suffer from setup uncertainties and from measure or modelling errors; (ii) even small disturbances are expected to involve dramatic changes in the measured/simulated flow because of the inherent chaotic nature of the turbulence. Hence, statistics over a sufficiently large number of realisations of the flow (obtained by means of both approaches) is to be preferred to a single measurements or simulation. Hence, the BARC differs, for instance, from the pioneering benchmark on the aerodynamics of the square cylinder [see for the review of the obtained results Rodi , 1997, Rodi, 2002, Voke, 1997], included since the Nineties in the ERCOFTAC classic collection database [Ercoftac test case LES2] and now in the ERCOFTAC QNET-CFD Knowledge Base Wiki [Ercoftac UFR2-02]. Indeed, this benchmark used as a reference the measurements by Lyn et al. [1995]. From this perspective, both computational simulations and wind tunnel tests provide single realisations of the flow. Moreover, the BARC aims at making available at its maturity a statistic database, which is expected to be further enriched and updated by new realisations.
At present, 78 participants in 43 teams are registered to access the web site member area (`http://www.aniv-iawe.org/barc`). Most of the participants come from academia (70%) and from research centres (19%), with smaller percentages coming from the consultancy (9%) and the industry (2%).
During the first four years of activity, thematic sessions have been devoted to BARC at the 5th European and African Conference on Wind Engineering (EACWE, 2009, Florence), at the 5th International Symposium on Computational Wind Engineering (CWE, 2010, Chapel Hill) and at the 13th International Conference on Wind Engineering (ICWE, 2011, Amsterdam). The last thematic session hosted 9 contributions and a final synopsis and overview. Besides the contributions to the mentioned conference thematic sessions, four journal papers explicitly referring to BARC have been published up to now [Bruno et al., 2010, 2012, Mannini et al., 2010, 2011].
Besides this introduction, the paper is organized into four more sections. In Section 2, the test case main setup and the result format required to the participant are recalled. In Section 3 the wind tunnel tests and the computational simulations performed up to now are described; their results are then compared in Section 4., which is further divided in three subsections: Sec. (4.1) deals with the analysis of the flow bulk parameters, the main flow features and statistics are described and compared in Sec. (4.2), while pressure and force correlations are reported in Sec. (4.3). Finally, in Section 5 some preliminary conclusions are attempted and further research perspectives are briefly sketched.

## 2 Test case main setup and result format

As mentioned in the Introduction, BARC addresses the high Reynolds number, external, unsteady flow over a stationary, sharp-edged smooth rectangular cylinder, and the associated aerodynamic loads [Bartoli et al., 2008a]. The breadth ($B$) to depth ($D$) ratio is set equal to 5.
The following common requirements are set for both wind tunnel tests and numerical simulations:

- the depth-based Reynolds number $\mathrm{Re}_D = UD/\nu$ has to be in the range of $2 \times 10^4$ to $6 \times 10^4$;
- the incoming flow has to be set parallel to the breadth of the rectangle, i.e. $\alpha = 0$, $\alpha$ being the angle of attack;
- the maximum intensity of the longitudinal component of the freestream turbulence is set to $I_x = 0.01$;
- the minimum spanwise length of the cylinder for wind tunnel tests and 3D numerical simulations is set to $L/D = 3$;

The following additional requirements are specified for wind tunnel tests:

- the maximum acceptable radius of curvature of the edges of wind tunnel models is set to $R/D = 0.05$;
- the maximum wind tunnel blockage is set to 5%;
- all the points of measurement have to be outside the boundary layers developed at the tunnel walls;
- uniformity of the flow at all measurement points must be checked in the empty tunnel and appropriately documented.

In addition to the main setup described above, sensitivity studies are strongly encouraged. The following additional values of the parameters are suggested for both wind tunnel tests and numerical simulations:

- angles of incidence $\alpha = 1, 3, 6$;
- Reynolds number $\mathrm{Re}_D = 10^3, 10^4, 10^5, 10^6$;
- turbulence intensity $I_x = 0.02, 0.05, 0.10$.

The flow quantities presented in the following are made nondimensional by using the undisturbed flow field velocity $U$, the cylinder depth $D$ and the fluid density $\rho$, unless specified otherwise.
Data can be uploaded to the BARC website by registered participants. Setup information and output data requested for numerical simulations and wind tunnel tests are set in Requests for Computational Simulations [Bartoli et al., 2008b] and Requests for Wind Tunnel Tests [Bartoli et al., 2008c], respectively.

## 3 Description of the wind tunnel tests and computational studies

The Special Technical Session at ICWE13 hosted 9 original contributions, summarising the results obtained in 59 realisations of the flow, i.e. 18 wind tunnel tests in three different facilities [Bartoli et al., 2011, Bronkhorst et al., 2011, Shirato et al., 2011], and 41 computational simulations [Arslan et al., 2011, Bruno et al., 2011, Grozescu et al., 2011a, Mannini and Schewe, 2011, Ribeiro, 2011, Wei and Kareem, 2011]. The resulting database is complemented by the studies presented at the previous BARC thematic sessions [e.g. Schewe, 2009, Shirato et al., 2010], and the ones published in the recent past on international journals [Bruno et al., 2010, 2012, Mannini et al., 2010, 2011].

Most of the studies adopt incoming flow characteristics in accordance with the range prescribed by the BARC main setup (see Sect. 2) and/or with the ones suggested for the sensitivity studies [e.g. turbulence intensity and length scale in Shirato et al., 2010, 2011]. The adopted incoming flow features are summarized in Figure 1. As for the freestream turbulence intensity, all the

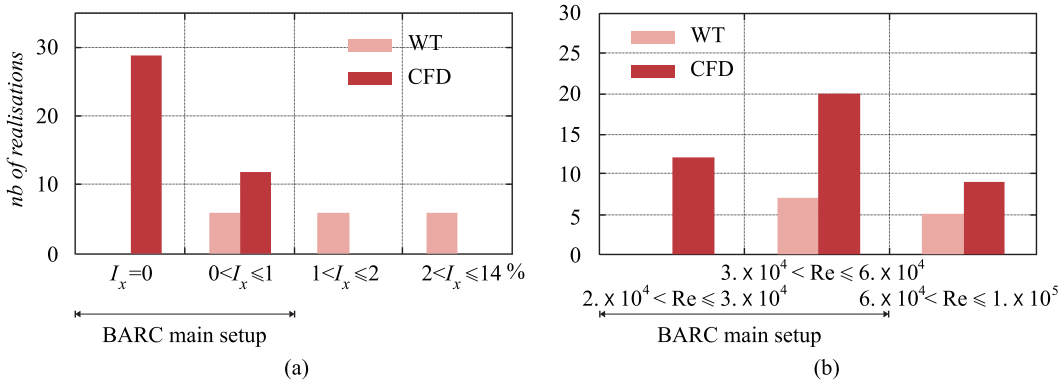


Fig. 1. Adopted incoming flow features: longitudinal turbulence intensity (a) and Reynolds number (b)

computational studies using Large-Eddy Simulation (LES) or Detached Eddy Simulation (DES) turbulence approaches adopt perfectly smooth incoming flow, mainly because of the difficulties involved in the generation of realistic incoming turbulence features within these approaches. Conversely, perfectly smooth flow conditions cannot be obtained in wind tunnels, where a residual turbulence always exists; on the other hand, grid turbulence generation is a relatively easy and inexpensive task in wind tunnel tests. Hence, the mentioned differences among computational and wind tunnel approach do not allow to compare flowfields obtained exactly in the same conditions, but the complementary features of each approach allow the effects of incoming turbulence to be investigated in a collaborative framework. Figure 1b also shows that another parameter significantly varying among the different contributions is the freestream Reynolds number, even if it keeps the same order of magnitude

and most of the values fall in the range specified in the BARC main setup. In the following subsections, the setup and objectives of both wind tunnel tests and computational simulations are shortly summarized. The given synopsis is intended to point out common and/or complementary features of the contributions to BARC rather than to detail each single study, for which interested readers are addressed to the original papers.

### *3.1 Wind tunnel tests*

The main characteristics of the setups of the wind tunnel contributions to BARC are given in table 3. Three of these contributions [Bartoli et al., 2011, Bronkhorst et al., 2011, Schewe, 2009] are aimed at obtaining measurements for freestream conditions that are as smooth as possible. Indeed, efforts are made to obtain a low freestream turbulence intensity and homogeneous inflow conditions. In particular, the contributions by [Bronkhorst et al., 2011] and [Bartoli et al., 2011] have to be considered calibration studies of the model and of the wind tunnel setup, and both point out the difficulties associated with obtaining a perfectly symmetric and two-dimensional configuration. In particular

Table 3
Wind tunnel tests: setup characteristics

| source | $\mathrm{Re}_D$ | $L/B$ | Blockage (%) | $I_x$ % | $L_x/D$ |
|---|---|---|---|---|---|
| Schewe [2009] | 26400 | 10.8 | 1.83 | 0.4 | – |
| Bronkhorst et al. [2011] | 50000 - 100000 | 4 | 3.5 | 0.32-0.56 | – |
| Bartoli et al. [2011] | 20000 -80000 | 7.93 | 3.75 | 1.6-2.1 | 1.27-1.87 |
| Shirato et al. [2011] | – | 3,6 | – | 10.5,11.5,14 | 0.92-3.16 |

several causes of asymmetry in the experiment conditions are identified and investigated, the main ones being the disturbances in the incoming flow, misalignment of the model with the incoming flow and inaccuracies in the model geometry. These three causes are separately analysed in [Bronkhorst et al., 2011]. The two research teams use different approaches when aligning the model in the wind tunnel. [Bartoli et al., 2011] use a trial and error approach, by rotating the model, horizontally placed in the wind tunnel, around its axis, and checking the value of the stagnation pressure coefficient. The tests are then carried out for the angle giving the largest value of the stagnation pressure coefficient, which turns out to be equal to 1. This approach allows compensating for possible flow non symmetries. [Bronkhorst et al., 2011], on the other hand, align the model, vertically placed in the wind tunnel, such to have its faces perpendicular to the tunnel walls (a turntable permits an accuracy of 0.05). This configuration brings a stagnation pressure coefficient of 1. In spite of the attention paid to the alignment of the model, both studies show a clear non symmetry in the mean and RMS pressure coefficients between the upper and lower faces. This issue will be discussed in details in Sec. 4.2.

In addition, [Bartoli et al., 2011] point out a deviation of the incoming flow when approaching the tunnel walls, which affects the spanwise distribution of the pressure statistics.
A different nature is that of the paper of Shirato et al. (2011), in which the characteristics of the spanwise coherence of the aerodynamic action of rectangular cylinders with B/D ratios ranging from 2.2 to 10 is investigated, for different intensity and scale of the incoming turbulence, obtained by means of three grid arrangements placed uspstream the model.
As for measurement techniques, pressure taps placed on the model surface are used in [Bartoli et al., 2011, Bronkhorst et al., 2011, Shirato et al., 2011] to provide the statistics of the pressure distribution at the body surface while unsteady aerodynamic loads are measured in [Schewe, 2009] by means of a high-stiffness piezoelectric balance.

### *3.2 Computational simulations*

The various numerical contributions differ for physical modeling, numerical methods and simulation set-up. We refer to the original papers for a complete description, while an overview is herein given of those aspects which have been the object of extensive sensitivity studies by the contributors.
A first issue is clearly turbulence modeling. The different numerical studies cover a wide range of approaches to turbulence (see Tab. 4), even if the studies based on LES and DES prevail over the ones using Unsteady Reynolds Average (URANS) models, the latter being restricted to the works of Mannini et al. [2010] and Ribeiro [2011]. LES simulations represent the 51% of the numerical contributions, the DES ones the 30% and, finally, URANS computations the 29%. Nevertheless, a significant number of URANS models have been applied to the test case, thanks to the affordable computational cost of each simulation: 1-equation SpalartAllmaras model (SA), Linearized Explicit Algebraic Wilcox $k-\omega$ model (LEA $k-\omega$), Menter $k-\omega$ model (SST $k-\omega$), realisable and RNG $k-\varepsilon$ models, Reynolds Stress Model (RSM). Testing the performance of the URANS approach is surely useful in an engineering perspective, as industrial applications often require simple and cheap 2D URANS simulations to investigate a large number of flow parameters and geometry configurations [e.g. in Ribeiro, 2011]. As for LES, both the classical formulation and the Variational Multi Scale one (VMS-LES) are tested in conjunction with a number of sub-grid models: Standard and Dynamic Smagorinsky Model (SM and DSM, respectively), Kinetic Energy one-equation model (KET), Wall-Adapting Local Eddy-viscosity (WALE) model. Finally, as for hybrid methods, both classical DES and Improved Delayed Detached Eddy Simulation (IDDES) are employed, where the SA model is adopted in the URANS part of the model. A more detailed description and the precise references for the adopted turbulence approaches and models can be found in the papers cited in Tab. 4.

Table 4
Computational studies: turbulence modeling

| | | turbulence model | |
|---|---|---|---|
| source | $\mathrm{Re}_D$ | approach | closures |
| Arslan et al. [2011] | $2.64 \times 10^4$ | LES | SM, DSM, KET |
| Bruno et al. [2010, 2011] | $4. \times 10^4$ | LES | KET |
| Grozescu et al. [2011a,b] | $2. \times 10^4, 4. \times 10^4$ | VMS-LES | SM, WALE |
| Mannini et al. [2010, 2011]; | $2.64 \times 10^4, 10^5$ | URANS | SA, LEA $k-\omega$ |
| Mannini and Schewe [2011] | | DES | SA |
| Ribeiro [2011] | $2.64 \times 10^4$ | URANS | RSM, SST $k-\omega$ |
| | | | real. and RNG $k-\varepsilon$ |
| Wei and Kareem [2011] | $10^5$ | LES | DSM |
| | | IDDES | SA |

As for numerical discretization, commercial codes [e.g. Fluent in Arslan et al., 2011, Ribeiro, 2011], opensource codes [Openfoam in Bruno et al., 2011, Wei and Kareem, 2011] and proprietary codes [Grozescu et al., 2011a, Mannini and Schewe, 2011] are used. All codes are based on the finite-volume method, except for the one used by Grozescu et al. [2011a], based on a mixed finite-element/finite-volume discretization. It is worth pointing out that only Mannini and Schewe [2011] address the effects of the numerical approach, and in particular of a tunable artificial dissipation term added to a central difference discretization of the convective fluxes.
As for the simulation set-up, the geometry of the spatial domain is characterized according to the BARC nomenclature given in Bartoli et al. [2008b] (Fig. 2). The values of the parameters adopted in each study are collected in Tab.

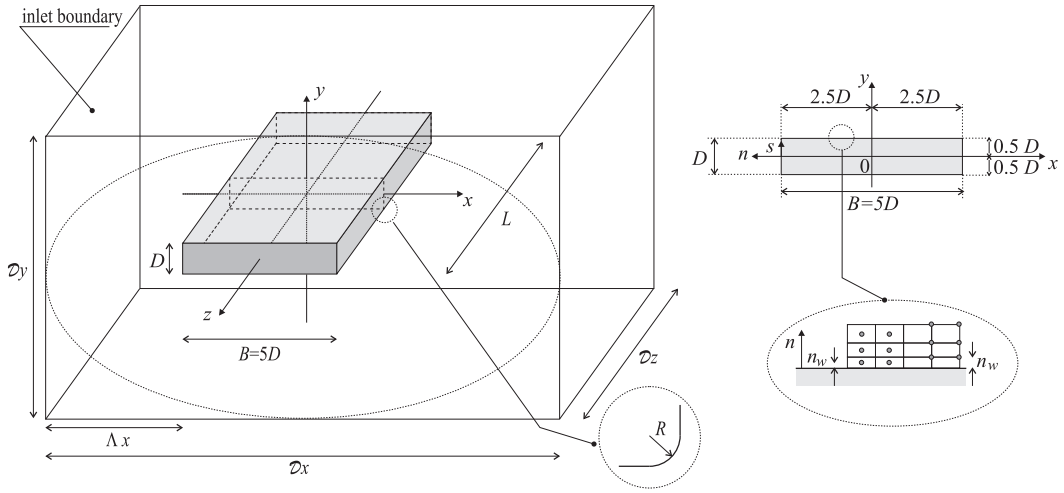


Fig. 2. Computational studies: model and domain geometry

5. Two-dimensional domains are adopted in 30% of the simulations in con-

Table 5
Computational studies: parameters of the computational domain

| source | dim. | shape | $\mathcal{D}_x/B$ | $\mathcal{D}_y/B$ | $\mathcal{D}_z/B$ | $\Lambda_x/B$ | $R/D$ |
|---|---|---|---|---|---|---|---|
| Arslan et al. [2011] | 3D | P | 23 | 20.2 | 1 | 10 | 0 |
| | 2D | P | 23 | 20.2 | – | 10 | 0 |
| Bruno et al. [2010, 2011] | 3D | P | 41 | 30.2 | 1,2,4 | 15 | 0 |
| Grozescu et al. [2011a,b] | 3D | P | 41 | 30.2 | 1 | 15 | 0 |
| Mannini et al. [2010, 2011]; | 2D | O | 200 | 200 | – | 100 | 0 |
| Mannini and Schewe [2011] | 3D | O | 200 | 200 | 1,2 | 100 | 0 |
| Ribeiro [2011] | 2D | O | 51 | 50.2 | – | 25 | $0 \div 0.1$ |
| Wei and Kareem [2011] | 3D | P | 8 | 3 | 0.2,0.4,1 | 1.5 | 0 |

junction with URANS models, except for a single LES simulation performed by Arslan et al. [2011] and aimed at comparing its accuracy with the 3D LES simulations in the same work. The shape of the domain is mostly prismatic (P) but cylindrical domains (O) are also generated by Mannini and Schewe [2011] and Ribeiro [2011], in concjunction with an O-grid in the latter study. In most cases, the domain dimensions in the $x$ and $y$ directions are about 20 to 50 times the breadth $B$ of the cylinder section, with remarkable exceptions in Mannini and Schewe [2011] ($\mathcal{D}_x/B = \mathcal{D}_y/B = 200$) and in Wei and Kareem [2011] ($\mathcal{D}_x/B = 8, \mathcal{D}_y/B = 3$): the former is expected to increase the computational cost but, of course, it avoids spurious effects of the boundary conditions on the simulated flowfield, while the domain size adopted in the latter is suspected to strongly affect the flow (see in particular the distance from the leading edge to the inlet $\Lambda_x/B = 1.5$). The cylinder spanwise length always corresponds to the domain size $\mathcal{D}_z/B$. The ensemble-average value of the latter is close to unit, but higher values are adopted in studies addressed to the evaluation of spanwise correlation [Bruno et al., 2011, Mannini et al., 2011], while shorter lengths are adopted by Wei and Kareem [2011].
As for the cylinder geometry, perfectly sharp edges are adopted in all cases, while Ribeiro [2011] also varies the radius of curvature of the edges of the cylinder in a broad range.
Tables 6 and 7 summarize some features of the generated spatial grids. Most of the grids are hybrid in the $x-y$ plane (i.e. body-fitted, structured in the near wall region and unstructured triangular or quadrilateral elsewhere), and structured along the spanwise direction $z$. Remarkable exceptions are the fully unstructured grids adopted by Grozescu et al. [2011a] and the structured ones used by Wei and Kareem [2011] (orthogonal) and Ribeiro [2011] (non orthogonal). Table 7 compares the grid spacing normal to the wall, and in the $x-$ and $z-$ directions. Most of the grids adopts $2. \times 10^{-5} \leq n_w/B \leq 5. \times 10^{-4}$ in order to obtain a grid resolution in wall units $\overline{n^+} \approx 1$, and to fully resolve the boundary layer without introducing wall-functions-like approximations. A large scatter is observed in the values of $\overline{\delta_x}/B$ : it is worth pointing out that the large value of $\overline{\delta_x}/B$ in Mannini and Schewe [2011] is justified by the

Table 6
Computational studies: grid type

| | | grid type | |
|---|---|---|---|
| source | dim. | $x$-$y$ plan | $z$-wise |
| Arslan et al. [2011] | 3D | hybrid | struct. |
| | 2D | hybrid | – |
| Bruno et al. [2010, 2011] | 3D | hybrid | struct. |
| Grozescu et al. [2011a,b] | 3D | unstr. | unstr. |
| Mannini et al. [2010, 2011]; | 3D | hybrid | struct. |
| Mannini and Schewe [2011] | 2D | hybrid | – |
| Ribeiro [2011] | 2D | struct. | – |
| Wei and Kareem [2011] | 3D | struct. | struct. |

Table 7
Computational studies: grid resolution

| source | $n_w/B$ | $\overline{n^+}$ | $\overline{\delta_x}/B$ | $\delta_z/B$ |
|---|---|---|---|---|
| Arslan et al. [2011] | $2. \times 10^{-4}$ | 0.5 | $4. \times 10^{-3}$ | 0.04 |
| Bruno et al. [2010, 2011] | $5. \times 10^{-4}$ | 1.66 | $2. \times 10^{-3}$ | 0.042÷0.01 |
| Grozescu et al. [2011a,b] | $5. \times 10^{-4}$, $2.5 \times 10^{-4}$ | ≈1 | 1.e-2, 5.e-3 | 0.042, 0.01 |
| Mannini and Schewe [2011] | $5. \times 10^{-5}$ | 0.25 | $1.4 \times 10^{-2}$ | 0.0156 |
| Ribeiro [2011] | 4.e-5 | ≈1 | 2.e-3 | – |
| Wei and Kareem [2011] | n.a. | 0.9÷7.44 | $10^{-2} \div 3.3 \times 10^{-3}$ | 0.04÷0.0025 |

DES model, while the one of the coarsest grid in Grozescu et al. [2011a] has been conceived to test the VMS-LES accuracy in conjunction with very coarse grids. The spanwise grid resolution varies from $\delta_z/B \approx 1/24$ in coarse grids to $\delta_z/B \approx 1/100$ in refined grids, with the remarkable exception of an even smaller grid step adopted by Wei and Kareem [2011].
The overall number of grid cells varies over 4 orders of magnitude among the studies (Fig. 3a), mainly depending on the approach to turbulence, the domain dimension and size, the grid type. Nevertheless, most of the models adopt an overall number of cells around one million (Fig. 3b). Only Bruno et al. [2010] provide some quantitative information about the cell skewness in the generated unstructured grid.
As for the inflow conditions, the numerical contributions cover different values of freestream turbulence intensity and Reynolds number(see Tab. 4 and Fig. 1). Nonetheless, explicit sensitivity studies are carried out only for the Reynolds number in Mannini et al. [2010], Grozescu et al. [2011a] and Grozescu et al. [2011b].

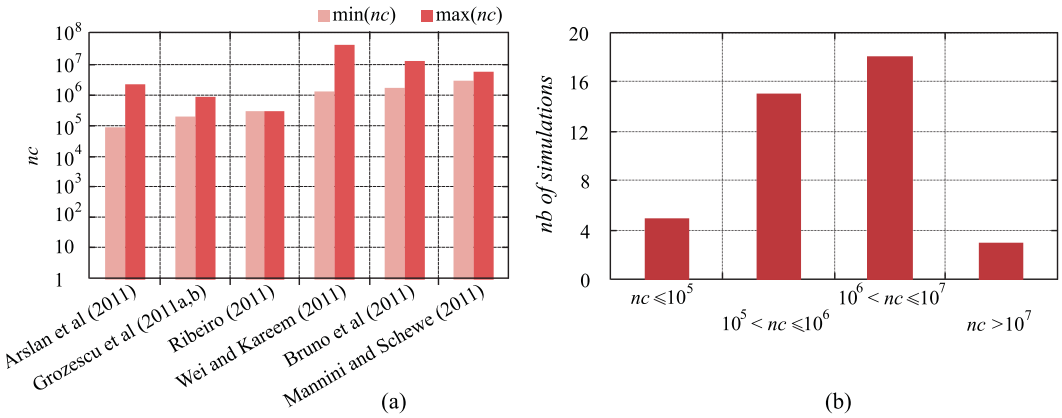


Fig. 3. Computational studies: number of cell for each study (a) and its overall distribution (b)

## 4 Comparison of the obtained results

For the sake of clarity, in the following the obtained results are schematically arranged in three subsections. The bulk paramenters are compared in the first subsection, the main statistical quantities characterizing the flow and the aerodynamic load distribution over the cylinder surface are discussed in the second one, while the third one is devoted to pressure and force spanwise correlation. Because of the considered time-dependent flow, statistics in time of the above mentioned quantities are performed by all the authors. The convergence of the obtained statistical moments of each quantity versus the sampling time should be addressed in order to avoid systematic postprocessing errors. In particular, the extent of the sampling window is a key and critical element in the CFD approach, due to the computational costs involved in long physical time simulations. Most of the authors [Arslan et al., 2011, Bronkhorst et al., 2011, Bruno et al., 2011, Grozescu et al., 2011a, Mannini et al., 2011, Wei and Kareem, 2011] check the convergence of the first and/or second order statistical moments of the bulk parameters. The minimum extent of the sampling window which allows convergence residuals below a given threshold for a given statistical moment is quantitatively evaluated in some works [Bronkhorst et al., 2011, Bruno et al., 2011, Grozescu et al., 2011a] by adopting the method proposed in Bruno et al. [2010]. The required sampling window depends on the simulated flow and hence on the experimental setup and model parameters, on the quantity to be statistically studied (e.g., for the studied flow, statistics of the Strouhal number converge faster than the ones of the lift coefficient), and, finally, on the order of the statistical moment to be evaluated. Nevertheless, some rough and indicative values follows from studies: a sampling extent longer than 400 non-dimensional time units is recommended to evaluate first-order statistical moments (time-averaged values); at least 900 non dimensional time units are required to obtain reasonably converged values of the second-order statistical moments.

### *4.1 Bulk parameters*

The main flow bulk parameters obtained in the different wind tunnel and numerical studies are reported in Tables 8 and 9: $t-avg(C_D)$ and $t-avg(C_L)$ are the time- and spanwise-averaged drag and lift coefficients per unit length, respectively; $t-std(C_L)$ is the standard deviation of the time variation of the lift coefficient; $St_D = f_s D/U$ is the Strouhal number, where the shedding frequency $f_s$ is evaluated from the time fluctuations of the lift coefficient or from pressure or velocity time signals (we refer to the single cited articles for more details).

First of all, we remark that at present, among the different wind tunnel tests carried out in the framework of the BARC benchmark, bulk parameters are available only from Schewe [2006, 2009] and from Bartoli et al. [2011] (only the Strouhal number). In general, several wind tunnel data are available in the literature for the flow around the same body geometry as far as the Strouhal number is concerned and only a few for the mean drag coefficient; these data are also reported in Table 8 for comparison. Conversely, bulk-parameter values computed in 25-36 simulations of the BARC configuration are available. The histograms of the bulk parameters obtained by computational simulations are plotted in Fig. 4. For the sake of brevity, detailed values are not given herein (we refer to the cited papers) and only the range of the results obtained in all the simulations carried out in each single contribution is reported in Table 9, together with the ensemble average over all the available data, the standard deviation and the minimum and maximum deviations, these two last quantities being given in percent of the ensemble average.

The values of $t-avg(C_D)$ obtained in most of the simulations are very close to

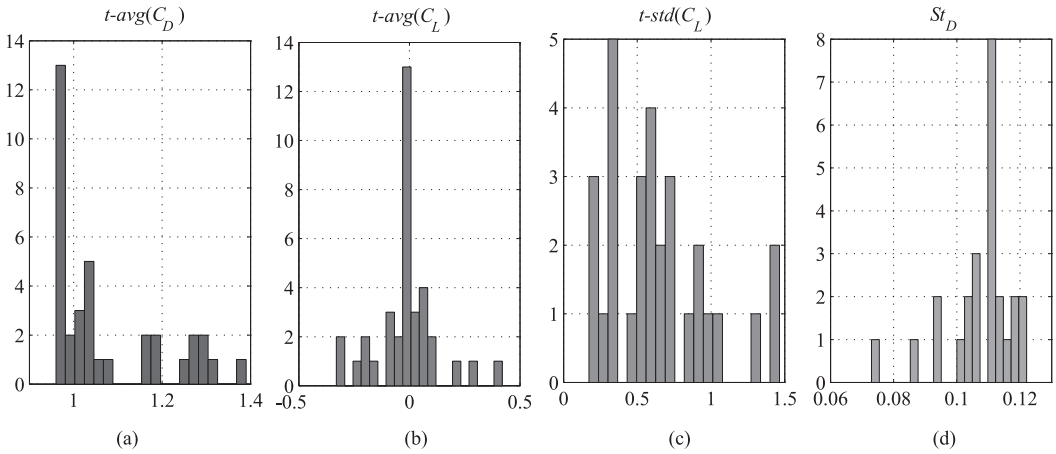


Fig. 4. Computational results: histograms of the bulk parameters; (a) $t-avg(C_D)$ over 36 realizations, (b) $t-avg(C_L)$ over 36 realizations, (c) $t-std(C_L)$ over 30 realizations, (d) $St$ over 25 realizations.

1 and this is in good agreement with the available wind tunnel data. Moreover, an overall good agreement is observed between the predictions obtained in

the various numerical studies, in spite of the previously outlined differences in numerics, modelling and simulation set-up. Indeed, the standard deviation of the data remains lower than 12% of the ensemble-averaged prediction. It will be shown in the following (Sec. 4.2) that, although the characteristics of flow on the cylinder sides significantly vary among the different simulations, the near-wake structure and, consequently, both the base mean pressure (see Fig. 5b) and the mean drag coefficient, show only small differences. Nonetheless, note that the maximum deviation of $t-avg(C_D)$ from its ensemble average is rather large; the largest values of $t-avg(C_D)$ are found in a 2D LES in Arslan et al. [2011] and in the LES and hybrid RANS/LES simulations in Wei and Kareem [2011]. The results of 2D LES could be expected to be rather unreliable, while, as for the simulations in Wei and Kareem [2011], characterized by very fine grid resolutions, the prediction of $t-avg(C_D)$ might be affected by the small extent of the computational domain in the lateral direction (see Tab. 5) and, therefore, to blockage effects.

The Strouhal number is another quantity for which the predictions given in the different simulations are rather close to each other and in good agreement with the available wind tunnel data. Since $St_D$ gives the dimensionless frequency of the vortex shedding behind the cylinder, this is a further confirmation that the dynamics of the near wake is satisfactorily captured in all the simulations in spite of the differences in the flow features on the cylinder lateral sides.

Conversely, the oscillations in time of the lift coefficient are very sensitive to the complex dynamics of the flow on the lateral cylinder sides. Indeed, a large spread of the numerical predictions is observed for the standard deviation of the lift coefficient. Note how the ensemble average of $t-std(C_L)$ obtained in the different simulations is significantly larger than the only available wind tunnel value (Tab. 8).

Finally, the mean lift coefficient is a-priori expected to be zero. Although values of $t-avg(C_L)$ close to zero are obtained in most of the simulations, there are a few cases in which its absolute value is significant (Bruno et al. [2011] and Wei and Kareem [2011]). This might be due to the fact that the time interval used to compute the averaged quantities is not large enough to obtain statistical convergence. Nonetheless, in Bruno et al. [2011], a careful check of the convergence of the averaged quantities is made, and, hence, at least in that case, the statistical sample may be assumed to be adequate. Therefore, it may be argued that a $t-avg(C_L)$ value significantly different from zero is an indication of an asymmetry of the mean flow which may be triggered into the analysed flow configuration by very small preturbations of different nature. This point will be more deeply analysed in Sec. 4.2.

Table 8
Bulk parameters: wind tunnel data

| | $t-avg(C_D)$ | $t-avg(C_L)$ | $t-std(C_L)$ | $St_D$ |
|---|---|---|---|---|
| Bartoli et al. [2011] | – | – | – | 0.12 |
| Schewe [2006, 2009] | 1.029 | $\sim 0$ | $\sim 0.4$ | 0.111 |
| Nakamura and Mizota [1975] | $\sim 1$ | – | – | – |
| Nakamura and Yoshimura [1982] | $\sim 1$ | – | – | – |
| Nakamura and Nakshima [1986] | – | – | – | 0.115 |
| Nakamura et al. [1991] | – | – | – | 0.118 |
| Okajima [1982] | – | – | – | 0.115 |
| Okajima [1983][1] | – | – | – | 0.105 |
| Parker and Welsh [1983] | – | – | – | 0.105 |
| Stokes and Welsh [1986] | – | – | – | 0.105 |
| Knisely [1990] | – | – | – | 0.106 |
| Matsumoto [2005][1] | $\sim 1$ | – | – | 0.132 |
| Ricciardelli and Marra [2008] | – | – | – | 0.116 |

[1] Reported in Mannini et al. [2011]

Table 9
Bulk parameters: numerical results

| | $t-avg(C_D)$ | $t-avg(C_L)$ | $t-std(C_L)$ | $St_D$ |
|---|---|---|---|---|
| Arslan et al. [2011] | 0.984–1.39 | – | 0.59–0.84 | 0.07–0.16 |
| Mannini et al. [2011] | 0.968 – 1.071 | 0.0032–0.047 | 0.42–1.075 | 0.094-0.102 |
| Mannini et al. [2010] | 1.015–1.172 | – | 0.108-1.12 | 0.087–0.105 |
| Mannini and Schewe [2011] | 0.965–1.016 | -0.087–0.085 | 0.173–0.553 | 0.087–0.119 |
| Ribeiro [2011] | 1.17 | – | 0.9 | 0.073 |
| Grozescu et al. [2011b] | 0.97–0.98 | -0.097–0.0043 | 0.52–0.65 | 0.107–0.11 |
| Grozescu et al. [2011a] | 0.96 | 0.0022 | 0.35 | 0.122 |
| Bruno et al. [2011][1] | 0.96 – 1.03 | -0.315– -0.0024 | 0.2–0.73 | 0.112–0.122 |
| Bruno et al. [2010] | 1.03 | – | 0.73 | 0.112 |
| Wei and Kareem [2011] | 1.165–1.305 | -0.33–0.42 | 0.495–1.465 | – |
| Ensemble average | 1.074 | -0.0141 | 0.65 | 0.109 |
| Maximum deviation: positive[2] | + 29.4% | +156.5 % | +125.4% | +11.6% |
| Maximum deviation: negative[2] | -10.6 % | -122.6 % | -73.4% | -33.3% |
| Standard deviation | 0.129 | 0.142 | 0.374 | 0.015 |
| Shimada and Ishihara [2002] | 0.975 | – | 0.03 – 0.12 | 0.103-0.119 |

[1] Also in Grozescu et al. [2011a]
[2] In percent of the ensemble-average value

### *4.2 Main flow features and statistics*

The distribution of the pressure coefficient $Cp$, averaged in time ($t-avg$ in the following), in the spanwise direction ($z-avg$ in the following) and between the upper and lower half perimeters ($side-avg$ in the following), is plotted in Fig. 5. Figure 5(a) collects the wind tunnel measurements, while Figure 5(b) the computational results. It is worth pointing out that Figure 5(a) (and Fig. 8(a) in the following) also includes the data obtained in high turbulent incoming flows by Le et al. [2009] for sake of completeness, even if the experimental setup significantly differs from the BARC main one.
As a first remark, the mean pressure values given by the different wind tunnel and computational contributions to BARC on the rear side of the cylinder are very close to each other and in good agreement with the experimental data available in the literature (also reported in Fig. 5(a)), with the only exception of the RANS computation with the RSM model in Ribeiro [2011]. As already mentioned in Sec. 4.1, this leads to very similar predictions of the time averaged drag.
Conversely, a significant spread of both wind tunnel and computational pres-

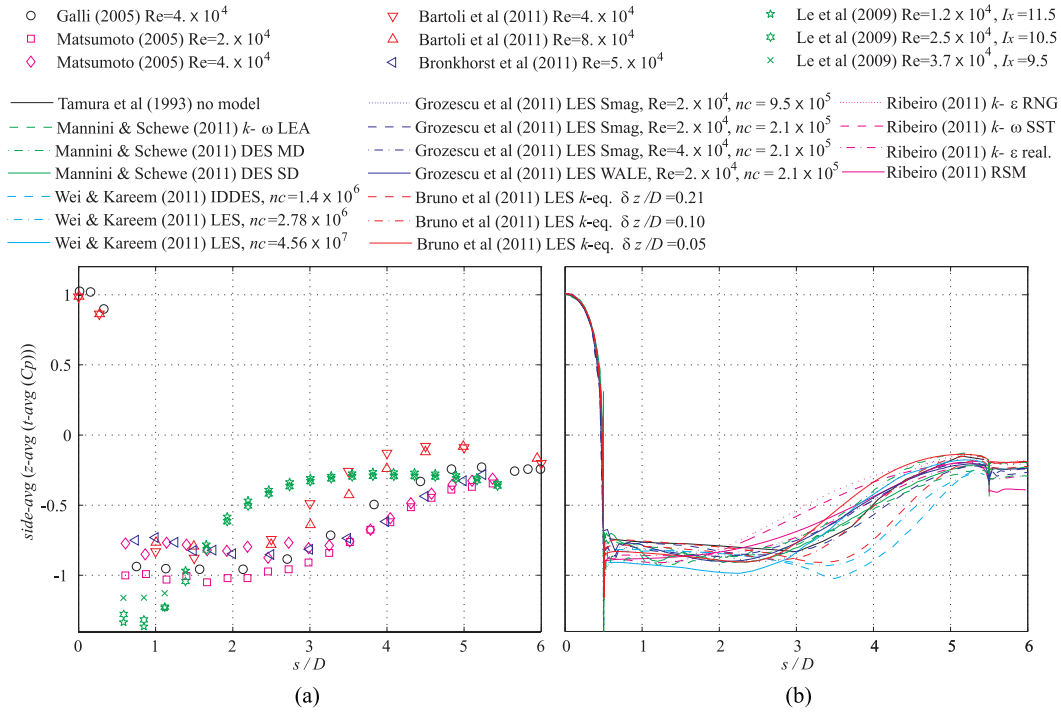


Fig. 5. Side-averaged, spanwise-averaged and time-averaged $Cp$ distributions: wind tunnel (a) and computational (b) results

sure values is observed in Fig. 5 on the lateral side of the cylinder. Figure 6 summarizes the ensemble statistics of the $C_p$ distributions on the lateral cylinder side; in particular, the range of the wind tunnel and numerical $C_p$ values is reported for 24 locations over the cylinder lateral side, together with

the median, the 25-th and the 75-th percentile values $p_{25}$ and $p_{75}$, respectively, whiskers and outliers, if any. Points are drawn as outliers if they are larger than $p_{75} + w\,(p_{75} - p_{25})$ or smaller than $p_{25} - w\,(p_{75} - p_{25})$, being $w = 1.5$ the maximum whisker length.

It is worth pointing out that the subset of wind tunnel pressure data over which statistics are evaluated does not include the realisations obtained in high turbulent incoming flows [Le et al., 2009], because such measurements do not belong to the same ensemble of smooth conditions. This holds also for the statistics of the standard deviation in time of the $Cp$ (Fig. 9).

As for the wind tunnel data, the distributions in Bartoli et al. [2011] are rather far from the remaining ones, which conversely well agree betweeneach other. As for the numerical results, although most of the distributions are contained in a narrower range than the wind tunnel one (Figure 6), the shape of the mean pressure distribution significantly varies among the different simulations. The spread in the predictions of the mean pressure distribution is strictly linked with the differences in the mean flow topology obtained in the various simulations (see Fig. 7). Therefore, before analysing in more detail the behaviour of the mean pressure coefficient on the cylinder lateral size, let us illustrate the main features of the mean flow topology emerging from Fig. 7.
The mean flow on the cylinder lateral side is characterized by a main recirculation zone (or main vortex as in Bruno et al. [2010]), whose size and shape significantly vary in the different contributions. To give a more precise quantification of this variability, Table 10 shows the $x$ coordinate at which the mean recirculation zone ends (mean reattachment location $x_r$) and the coordinates of the centre of the main recirculation zone. Only a subset of the contributions to BARC, for which these data were made available, is considered; as previously for the bulk coefficients, detailed values are not given in Table 10 for the sake of brevity (we refer to the cited papers), and only the range of the results obtained in all the simulations carried out in each single contribution is reported, together with the ensemble average and the standard deviation over all the available data. The value of $x_r$ deduced by Matsumoto et al. [2003] from wind tunnel pressure measurements is also shown for reference. The data in Tab. 10 confirm a significant variability of the length and of the $x$ position of the centre of the mean vortex, while the normal distance from the cylinder of its centre remains almost constant. This leads to very different shapes and curvature of the mean streamlines at the edge of this main recirculation zone. It is not easy to identify a trend with the different simulation parameters; for instance, 2D no-model and LES simulations lead to a very short main vortex, while 2D RANS simulations may yield long main vortices depending on the turbulence model. From the results of Bruno et al. [2011] and Grozescu et al. [2011a,b], it seems that grid refinement leads to a decrease of the main vortex length and to an upstream displacement of its centre. Finally, a strong impact of the numerical dissipation is observed in the DES simulations in

Mannini and Schewe [2011], the length of the main recirculation zone becoming smaller with decreasing numerical dissipation. In most of the numerical contributions to BARC (Fig. 7), a smaller recirculation is also visible very close to the lateral wall and immediately downstream of the upstream corner, which was already detected in Bruno et al. [2010] (see in particular Fig. 11 of Bruno et al. [2010], in which the mean flow structures are sketched). Again, its dimensions and shape vary significantly among the different simulations; in fact, in some cases it is hardly visible. From the results of Bruno et al. [2011] and Grozescu et al. [2011a,b], it appears that the size of thissmaller recirculation region increases with grid refinement, while it is hard to identify a trend with the remaining simulation parameters.
Coming back to the analysis of the mean $C_p$ behaviour (Fig. 5), for all experiments and simulations adopting smooth and low turbulence incoming flow a first zone of almost constant low pressure can be observed; the length of the pressure coefficient plateau roughly corresponds to the distance from the upstream corner to the centre of the main vortex. In this first zone, rather surprisingly, the spread of the numerical results is lower than that of the wind tunnel ones. This may be due to the fact that in this upstream part of the lateral side, in spite of the previously analysed significant differences in the mean flow topology, the curvature of the mean streamlines is similar for all the simulations (Fig. 7). More downstream, in all cases the pressure increases again because of the change in the curvature of the mean streamlines as the mean flow tends to reattach (see Fig. 5). This is the region in which the largest spread among the different datasets is observed, in particular in the position at which the pressure starts to increase and in the steepness of the positive gradient (Fig. 5). Considering that the normal distance from the side surface to the centre of the vortex does not vary significantly (see Tab. 10 and the related discussion), in general a shorter recirculation zone leads to a larger curvature of the mean streamlines, which in turn implies a more rapid increase of the mean pressure coefficient.
The distribution of the standard deviation of the time variation of the $Cp$ pressure coefficient, averaged also spanwise and between the upper and lower half perimeters, is plotted in Fig. 8. As an overall remark, a large spread among the different experimental and numerical predictions of this quantity is evident. In this case the variability is larger for the numerical results than for the nd tunnel measurements, as also visualized in Fig. 9, in which the same statistics as in Fig. 6 are reported now for the $C_p$ standard deviation. More particularly, on the upstream side of the cylinder the $C_p$ standard deviation is very low in all the numerical simulations, while in most of the experiments is roughly around 0.05. This may be explained by the difference in the free-stream conditions, which are smooth in most of the numerical simulations, while turbulent fluctuations are present in the experiments, although the turbulence intensity is kept low. As for its mean value, the largest variability $C_p$ standard deviationis observed on the cylinder lateral side. In all cases there is a peak located slightly upstream of the reattachment of the main mean

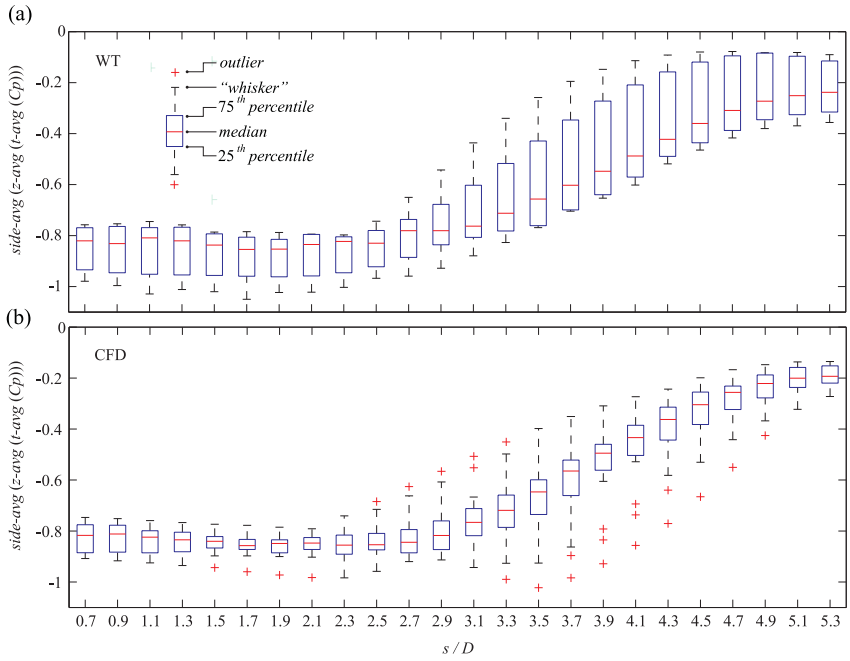


Fig. 6. Statistics of the side-averaged, spanwise-averaged and time-averaged $Cp$ distributions: wind tunnel (a, 6 realisations) and computational (b, 18 realisations) results.

recirculation vortex, in the zone where the mean $Cp$ increases. In average, the peak is located more downstream and is more intense in numerical simulations than in experiments (compare Figs. 9a and 9b). Since the approach to turbulence is expected to have a significant impact on the numerical predictions of this quantity, Figs. 9c and 9d compare the distributions of the standard deviation of $C_p$ obtained on the cylinder lateral surface in DES and LES simulations to those given by URANS models. Quite surprisingly the differences in the intensity and location of the main peak are rather small; therefore, it seems that turbulence modeling has an effect on the dynamics of the flow over the lateral cylinder sides which is comparable to that of other sources of uncertainties present in the simulations and experiments. The main difference is that in DES and LES simulations, consistently with the wind tunnel measurements, the value of the standard deviation of $C_p$ has an unique peak along the cylinder side, while in the RANS ones a minimum is also found at a distance of approximately 2D from the upstream corner. The reasons of this behavior are not clear at this stage. It is worth pointing out that the pressure coefficient distributions previously commented in the present section result from the averaging between the upper and lower half perimeters, so that possible asymmetries with respect to the $x$ axis can not be pointed out. In fact, the pressure measurements in wind tunnel tests [Bartoli et al., 2011, Bronkhorst et al., 2011] and some computational simulations [Bruno et al., 2012, Grozescu et al., 2011a] highlight emerging differences in the statistics of pressure fields over the upper and lower lateral surfaces. The difference and the absolute difference of the $t - avg(Cp)$ and $t - std(Cp)$ distributions between

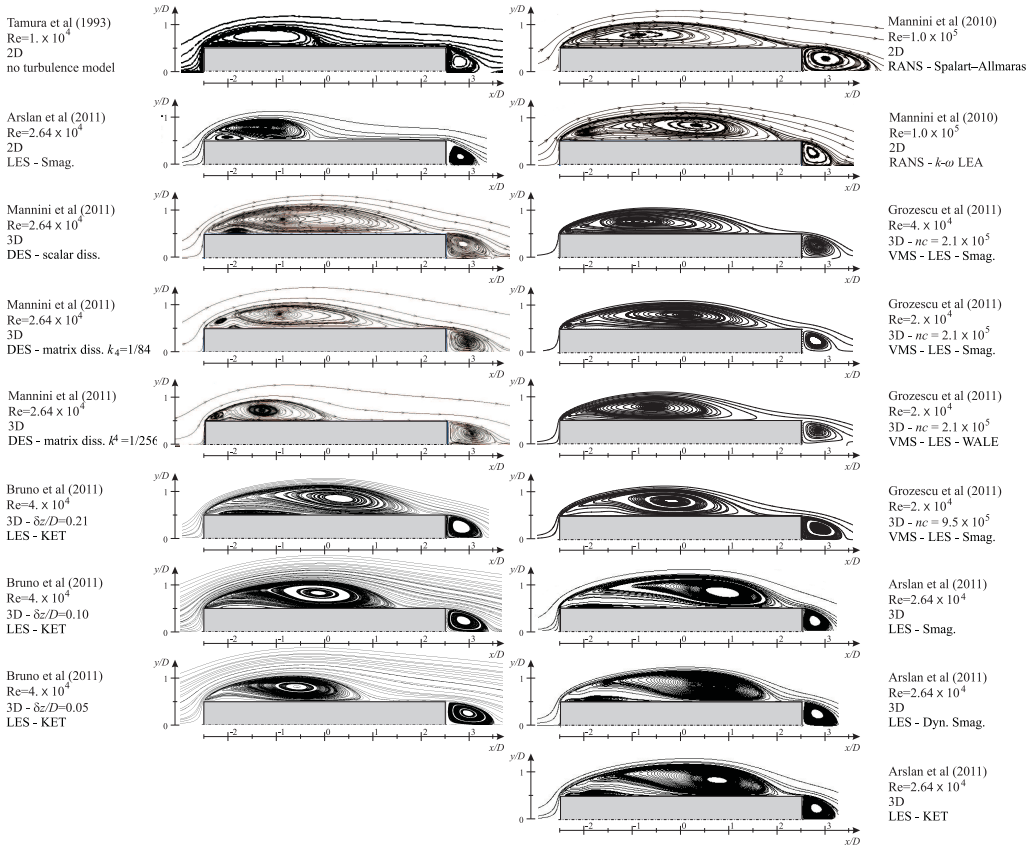


Fig. 7. Time and spanwise-averaged streamlines

Table 10
Mean reattachment location ($x_r$) and coordinates of the centre of the mean recirculation zone ($x_c, y_c$)

| | $x_r$ | $x_c$ | $y_c$ |
|---|---|---|---|
| Arslan et al. [2011] | $0.66 \div 2.29$ | $-1.24 \div 0.75$ | $0.78 \div 0.82$ |
| Mannini et al. [2011] | 2.25 | – | – |
| Mannini et al. [2009][1] | $1.72 \div 2.06$ | $-1.44 \div -0.05$ | $0.77 \div 0.88$ |
| Grozescu et al. [2011a] | $1.65 \div 2.1$ | $-0.97 \div 0.09$ | $0.76 \div 0.805$ |
| Grozescu et al. [2011b] | 1.64 | -0.17 | 0.35 0.82 |
| Bruno et al. [2010] | 2.18 | 0.04[1] | 0.8[1] |
| Ensemble average | 2.25 | -0.23 | 0.804 |
| Standard deviation | 0.45 | 0.73 | 0.033 |
| Matsumoto et al. [2003] | 1.875 | – | – |

[1] Reported in Arslan et al. [2011]
[2] In percent of the ensemble-average value

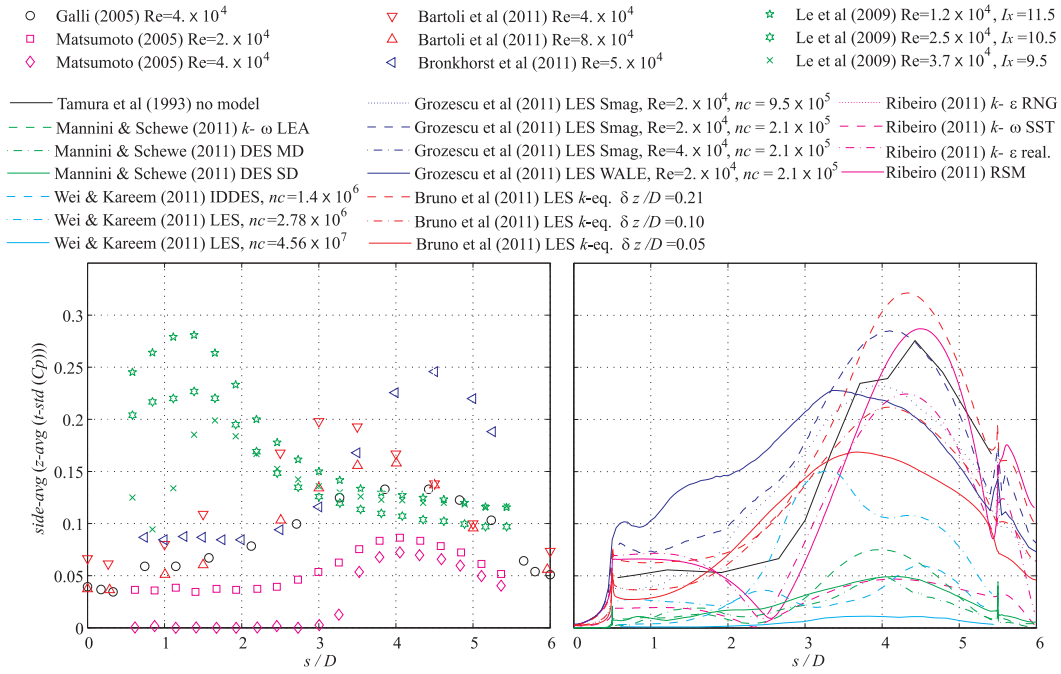


Fig. 8. Side-averaged, spanwise-averaged distributions of the standard deviation in time of the $Cp$: wind tunnel (a) and computational (b) results

the upper and lower half perimeters are shown in Figure 10 and Figure 11, respectively, for the cited studies. For a generic variable $\phi$, the difference is defined as $\Delta\phi = \phi(s/D) - \phi(12 - s/D)$, being $0 \leq s/D \leq 6$. In the same figure, also the corresponding boxplot statistic description is given. Significant differences between the upper and lower surfaces (up to$\Delta(t - avg(Cp)) \approx 0.1$ and $\Delta t - std(Cp) \approx 0.05$) are obtained in wind tunnel measurements and in some computational simulations. The distributions of the differences along the side surface show some common qualitative trends, i.e. they are not monotonic and they change sign along the central part of the lateral surface; in some cases, different authors obtain specular qualitative trend, i.e. a local maximum value of a distribution roughly corresponds to the minimum one in an other distribution and vice versa: compare for instance $\Delta(t - avg(Cp))$ in Bronkhorst et al. [2011] and Bartoli et al. [2011], or in Bruno et al. [2012] and Grozescu et al. [2011a]. As a consequence of these mirror-like, non monotonic distributions, the ensemble averaged value of the absolute differences has two maxima along the side surface at $s/D \approx 2.5$ and $s/D \approx 4.5$ (see fig. 11(d)), while the ensemble averaged value of the differences is close to zero at every location along the side surface, even if the number of realisations in the ensemble is quite low (see fig. 11(c)). Thus, in agreement with Carassale [2008], the ensemble-averaged flow around nominally symmetric setup is symmetric, also in case of non-ergodic phenomena. In other words, the average over a large-enough number of realisations of the flow around a nominally symmetric setup (e.g. obtained by wind tunnel tests or computational simulations) is symmetric, even if the time-average (and in this case spanwise averaged) flow in a single

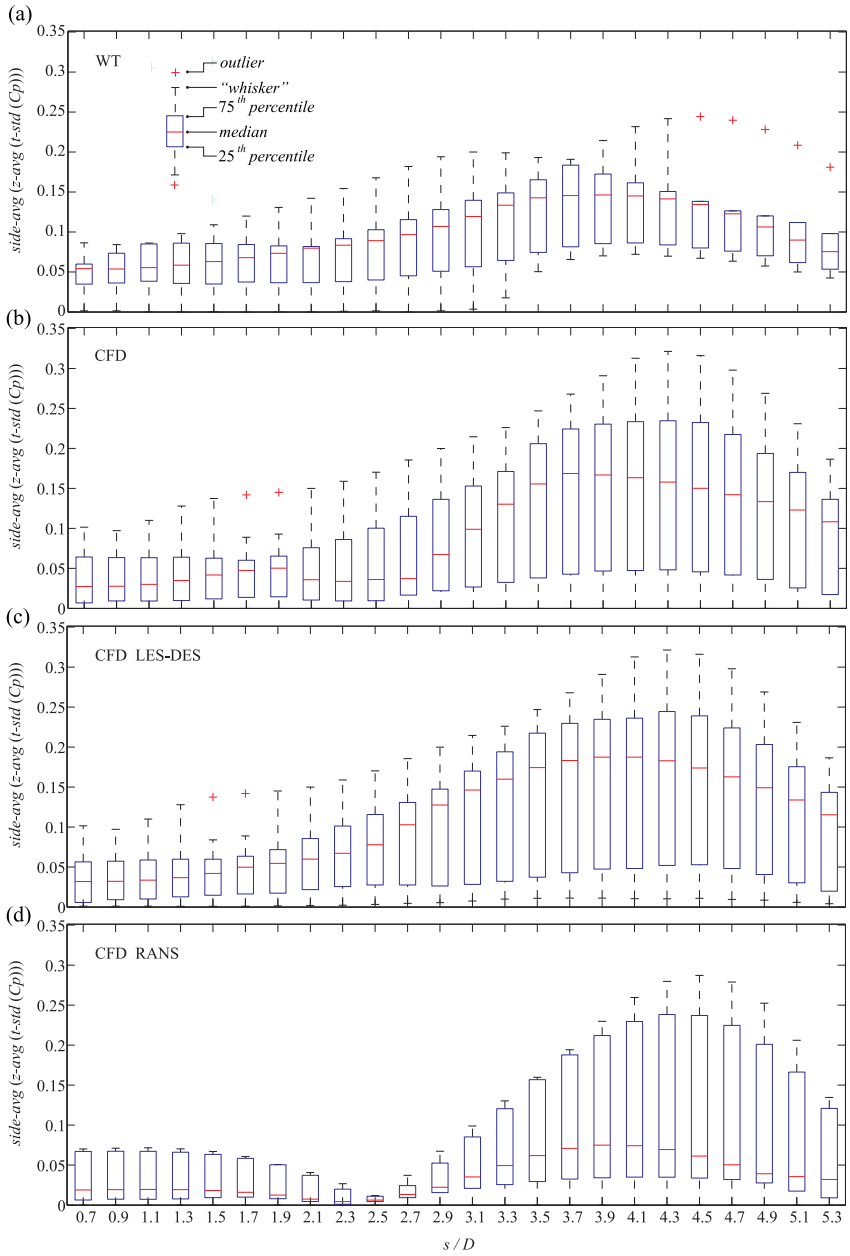


Fig. 9. Statistics of the side-averaged distributions of the standard deviation in time of the $Cp$: wind tunnel (a, 6 realisations) and computational (b, 18 realisations; c, 13 realisations; d, 5 realisations) results

realisation can be asymmetric.
Nevertheless, these findings do not shed light about the cause(s) of the occurence of single asymmetric flow realisations. Sistematic errors due to insufficient sampling window in time and related lack of convergence in evaluating the pressure statistical moment are avoided by convergence assessment, as described at the beginning of sect. 4.
In the preliminary wind tunnel studies by Bronkhorst et al. [2011] and Bartoli et al. [2011] different possible causes of the non-symmetry were identified, the main

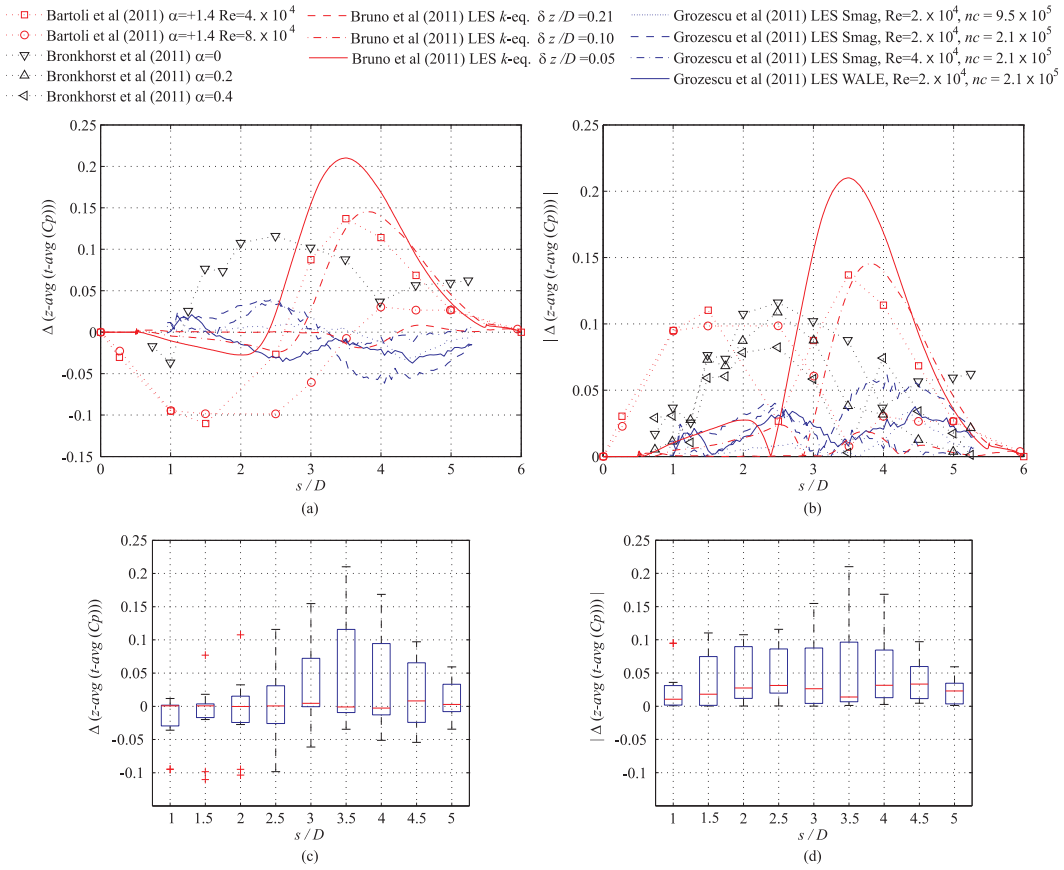


Fig. 10. Difference and absolute difference of the $t-avg$ pressure coefficient distributions along at the upper and lower half perimeters: realisations (a, b) and corresponding statistics (c,d).

being the disturbances in the incoming flow (e.g. by the upstream pitot-static tube), misalignment of the model with the incoming flow (e.g. misalignment of the model and/or asymmetry in the flow) and inaccuracies in the model geometry (e.g. degree of sharpness of the four edges, pressure taps disturbances and or quality of the rectangular shape of the model section). These three causes are separately and sistematically addressed in Bronkhorst et al. [2011], while Bartoli et al. [2011] focus on last ones. Based on the performed investigations, Bronkhorst et al. [2011] conjecture that the asymmetry results from an inaccuracy in model shape, while misalignment of the relative flow is tentatively suspected by Bartoli et al. [2011]. In spite of a number of trial re-alignments and model flippings, both studies do not obtain a perfect symmetry of the time-averaged pressure field along the side surfaces.
The computational models are not affected by the wind tunnel error sources. In particular, the mathematical model accounts for perfectly rectangular cylinder section with perfectly sharp edges, while the laminar incoming flow and the other boundary conditions are fully symmetric. Hence, asymmetric flow can be triggered only by numerical issues. Local asymmetries exist in the spatial grid generated by Bruno et al. [2012] outside the grid boundary layer at the wall,

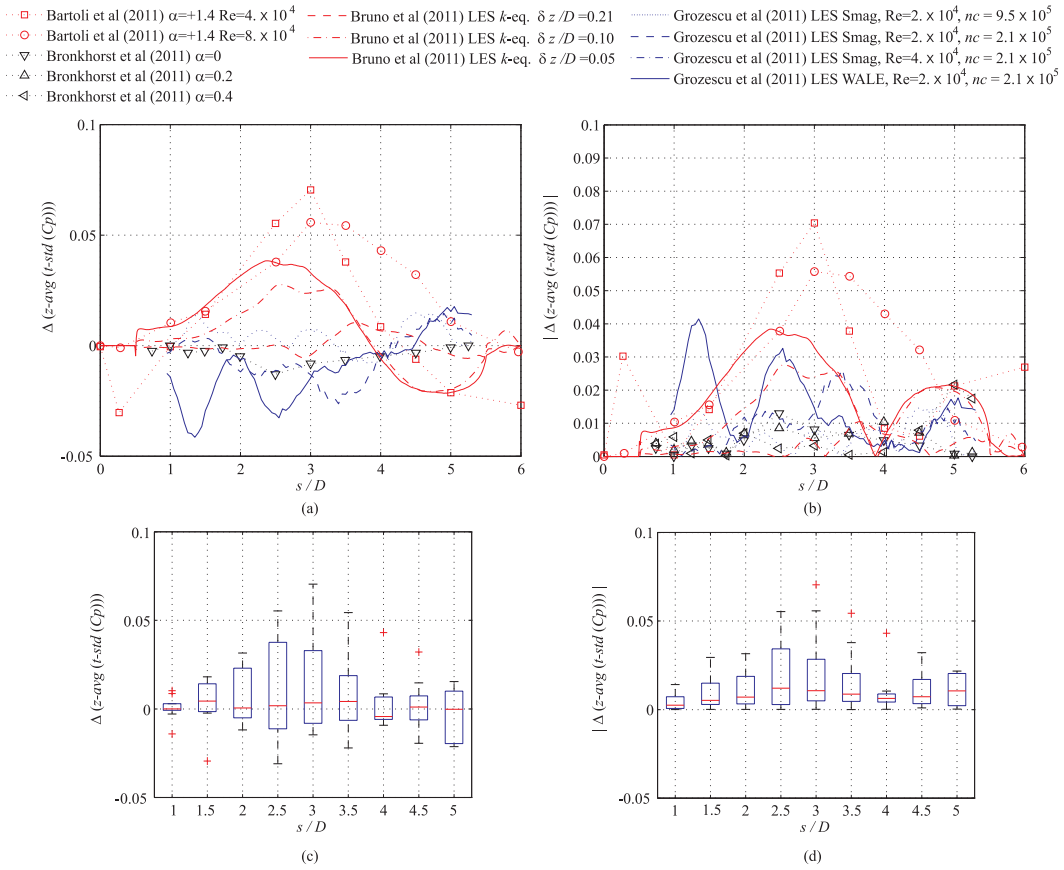


Fig. 11. Difference and absolute difference of the $t-std$ pressure coefficient distributions along at the upper and lower half perimeters: realisations and corresponding statistics

while the mesh generated by Grozescu et al. [2011a] is fully symmetric with respect to the $x-z$ plane. The procedures adopted for the numerical discretization and numerical solution of the governing equations (e.g. multigrid partition and parallelisation) can represent further potential causes of an asymmetric solution. The computational simulations performed by Grozescu et al. [2011a] provide smaller differences than the ones pointed out by Bruno et al. [2012]. Nevertheless, asymmetry in Grozescu et al. [2011a] is predicted by various subgrid models and holds at different Re numbers, even if a clear trend versus the latter can not be recognized. Conversely, the systematic grid refinement in the spanwise $z-$ direction performed in Bruno et al. [2012] suggests that the asymmetric time and spanwise averaged pressure field can be simulated only by using a dense grid, while negligible differences take place with the coarsest mesh. The authors conjecture that small coherent flow structures in the spanwise direction past the trailing edges are responsible of the whole asymmetric flowfield.

In general, the scrutinized studies show that the BARC flow has an high sensitivity to a number of factors which may trigger a significant asymmetry in the time-averaged flow field. It is worth recalling that some analogous well

known examples of time-averaged asymmetric flows around nominally symmetric setups exist in bluff body aerodynamics, e.g. the circular cylinder in its critical regime [Bearman , 1969, Schewe, 1983], or the side-by-side arrangement of two rectangular cylinders [$B/D = 1.28$, $S/D = 0.5$, where $S$ is the gap between cylinders, Matsumoto et al., 2008]. Another example, which is more similar to the flow setup discussed in this paper, is provided by Ohya et al. [1992], where the flow at $\mathrm{Re}_D = UD/\nu = 10^3$ around rectangular cylinders with different breadth to depth ratios ($3 \leq B/D \leq 9$) is simulated by solving the 2D Navier-Stokes equations without turbulence models. The simulated time-averaged flow is symmetric for all the considered $B/D$ ratios (included the one characterized by $B/D = 5$), except for $B/D = 4$. It is worth noting that this asymmetry is not revealed in previous wind tunnel tests performed by the same authors [Nakamura et al., 1991] under the same incoming flow conditions.
Summarizing, some of the above mentioned causes of asymmetry are connected with the set-up parameters which are uncertain in both wind tunnel tests and computational simulations. Therefore, robust procedures to set, evaluate and control parametric uncertainties in wind tunnel test could be detailed in a Best Practice guideline for these type of studies, as proposed by Bronkhorst et al. [2011] and probabilistic approaches can be useful to account for the setup uncertainties and to evaluate their propagation in the aerodynamic properties of bluff bodies [e.g. Bruno and Fransos, 2011, Han et al., 2012]. Further computational and wind tunnel investigations are also encouraged in the framework of the benchmark, e.g. addressed to evaluate the critical value of the setup parameters driving the instability or to show the existence of two post critical asymmetric solutions of the bi-stable flow induced by disturbances of opposite sign.

### *4.3 Pressure and force spanwise correlation*

This last subsection is devoted to the comparison of the spanwise correlation coefficient of pressure and forces. The spanwise correlation is necessary to accurately evaluate the actual overall wind loads on structures and their response. Therefore, the comparison of the spanwise correlation values obtained in the benchmark by means of different approaches and by different authors is a valuable complement to the comparisons shown in the previous sections. Note that the accurate simulation of the flow spanwise features is a very demanding task for the computational approach, mainly because of the requirements concerning the spanwise domain size and the grid density. While several studies have been devoted to the evaluation of the spanwise correlation in the case of the square cylinder [e.g. in McLean and Gartshore, 1992, Namiranian and Gartshore, 1988, Oka and Ishihara, 2009, Tamura et al., 1998, Vickery, 1966], the BARC benchmark gives a complement to a single study

[Ricciardelli, 2010] already available in the literature about the spanwise correlation in the case of the high Re flow around the rectangular 5:1 cylinder. In what follows, the spanwise correlation of a generic aerodynamic variable $C_i$ is described through its correlation coefficient

$$R_{C_i}\left(\Delta z/D\right) = \mathrm{cov}\left[C_i\left(\Delta z/D\right)\right]/\mathrm{var}\left[C_i\right] \tag{1}$$

where $\Delta z/D$ is the spanwise separation between two points at which the variable is measured.

The pressure correlation coefficients obtained in both wind tunnel tests [De Grenet and Ricciardelli, 2005, Ricciardelli and Marra, 2008] and computational simulations [Bruno et al., 2012, Mannini et al., 2011] along three spanwise alignments $si$, $1 \leq i \leq 3$ are compared in Figure 12 and their statistics are given in terms of boxplots. The alignments are selected in order to be rapre-

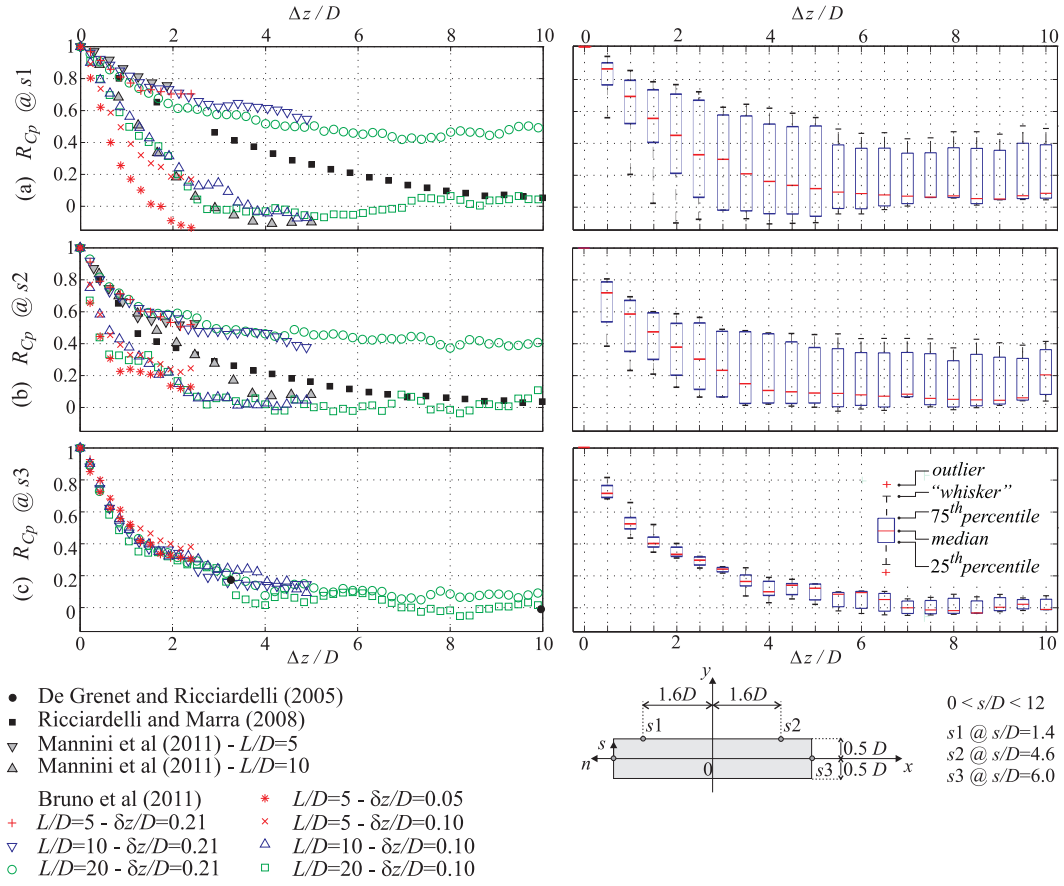


Fig. 12. Pressure correlation coefficients along three spanwise alignments: realisations and corresponding statistics

sentative of different flow regions, i.e. just downstream the separation point in the recirculation bubble ($s1$), close to the reattachment point ($s2$), and on the rear side ($s3$). The correlation coefficients of the lift and drag forces and their ensamble statistics are plotted in Figure 13. In particular, the lift correlation data include the wind tunnel measurements obtained by Shirato et al. [2010]

under turbulent incoming flow characterized by a vertical turbulence intensity of about 11% and by different values of the vertical scale of turbulence $L_y$ (for the other turbulence properties, see the cited paper). The pressure corre-

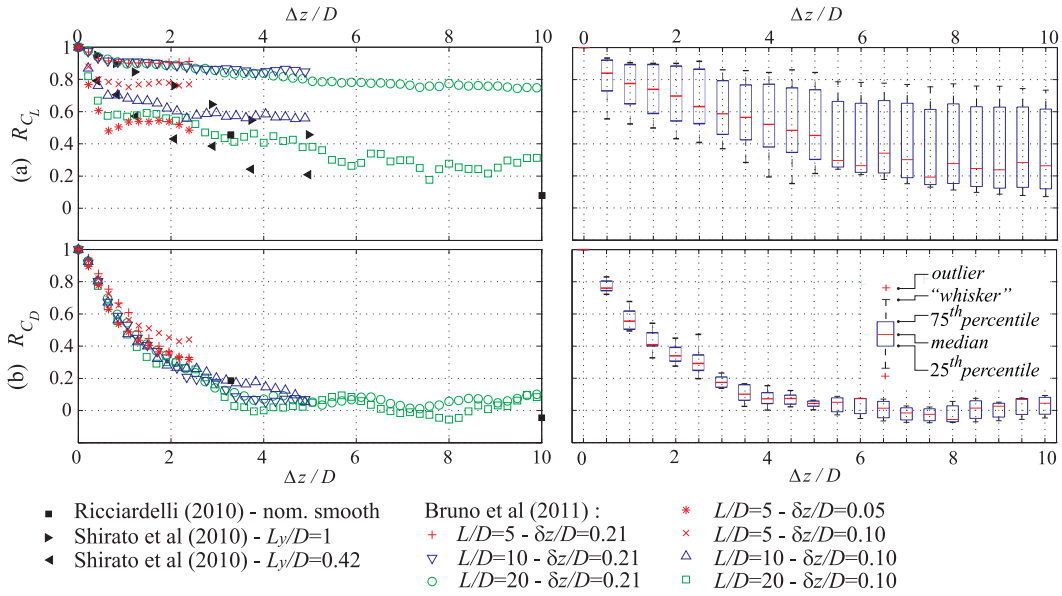


Fig. 13. Lift and drag correlation coefficients: realisations and corresponding statistics

lations at the rear surface (alignment $s3$) and the drag correlations obtained by different aproaches are in very good agreement among them, so that the ensamble of the results is characterized by a negligible deviation. Conversely, the collected data of the pressure correlation coefficent along the side surface (alignments $s1, s2$) are significantly dispersed. The same statistical trend holds for the data of the lift correlation coefficient, which mainly results from the pressure distribution of the side surface. This dispersion confirms the sensitivity of the 3D flow along the side surface to a number of model parameters (e.g. the spanwise grid density $\delta z$ and the domain length $L$ in computational simulations) and incoming flow conditions (e.g. the turbulence length scale in wind tunnel tests). In particular, a small spanwise grid step ($\delta z/D \leq 0.05$) seems to be required in LES simulations to achieve a satisfactory grid convergence. Furthermore, it is worth noting that the correlation coefficient predicted by LES and DES simulations along the alignment $s1$ takes negative values for $2 \leq \Delta z/D \leq 7$ before vanishing for larger values of the spanwise separation: a non monothonic trend of the correlation coefficient versus $\Delta z$ follows. A sound phenomenological interpretation of this result has not been provided in Bruno et al. [2012], Mannini et al. [2011], and further investigations are welcome in the BARC future activities. Finally, the correlation of the lift coefficient has also been described through the correlation length $L_L$, a sinthetic measure of the spanwise distance over which the sectional lift force can be

reasonably considered fully correlated. It can be expressed as

$$L_L = \int_0^\infty \tilde{R}_{C_L} \left(\Delta z/D\right) d\left(\Delta z\right), \tag{2}$$

where $\tilde{R}_{C_L} = exp\left[-c\Delta z/D\right]$ is the exponential function which best fits the lift correlation coefficient, and $c$ the decay coefficient. The lift correlation lengths available in BARC studies are plotted in Figure 14 versus a characteristic length of the model setup: the spanwise grid step $\delta z/D$ for LES simulations, the vertical scale of grid turbulence $L_y$ for wind tunnel tests. It is worth pointing out that the one reported in Ricciardelli [2010] is obtained in wind tunnel residual turbulence ($I_x \approx 0.02$): its vertical length scale ($L_y \approx 0.1$ [m], i.e. $L_y/B \approx 0.33$) has not been evaluated during the tests, and has been recovered by further tests in the same facility fully described in Bartoli et al. [2011]. The longer the characteristic length of the model setup, the longer

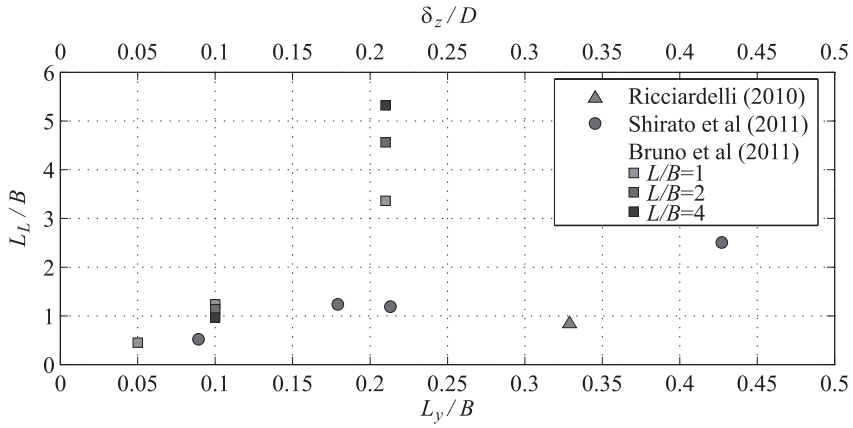


Fig. 14. Lift correlation length versus the spanwise grid density $\delta z$ and the vertical scale of turbulence $L_y$

the lift correlation length. In particular, a linear dependency between the lift correlation length and the vertical turbulence length scale has been recognized by Shirato et al. [2010], while an exponential-like growth of the lift correlation length versus the spanwise grid spacing can be recognized in the data by Bruno et al. [2012]. The analogous effects of the the vertical turbulence length scale in experiments and of the spanwise grid spacing in computations may be explained by the fact that these are the parameters mainly determining the characterisitic size of turbulence scales in the flowfield. In fact, the freestream turbulent length scale in wind tunnel tests is a direct measure of the size of main vortices in the incoming flow, while the grid size in LES simulation is an indirect measure of the size of the resolved turbulence scales in the flow after the transition induced by the obstacle (the incoming flow being laminar). Both the inflow vortical structures of experiments and the smallest eddies directly simulated in the trailing flow seem, therefore, to affect the spanwise correlation in the same way. A value of about $L_L/B \approx 0.5$ is expected for both wind tunnel tests with very small incoming vertical turbulence length scale

and computational simulations with perfectly smooth incoming flow and very small spanwise grid resolution.

## 5 Conclusions

An overview has been presented aimed at summarising and disseminating the research activity performed during the first four year of activity of the Benchmark on the Aerodynamics of a Rectangular 5:1 Cylinder. In this overview, the BARC flow has been first put in context of the scientific literature available at the benchmark launching. Then, wind tunnel measurements and the computational simulations provided by 10 research teams have been compared. The results obtained from nominally common setups have been collected in a single ensemble of realisations in order to obtain statistics of several flow quantitites, such as bulk parameters, chordwise pressure distributions, spanwise correlation. Some bulk parameters (e.g. the $St$ number) show narrow histograms, while others (e.g. the $t-std(C_L)$) are significantly dispersed. The $t-std(C_L)$ dispersion is recognized to be due to the high sensitivity of the flow along the side surface to small differences in the wind tunnel setup and in the simulation parameters. Consequently, the statistics of the pressure distribution on the cylinder lateral surfaces also show significant dispersion, both in wind tunnel measurements and in numerical simulations. Conversely, the wind tunnel measurements and the numerical predictions of base pressure, and, hence, of the drag have been found to be in overall very good agreement. The spanwise pressure correlation coefficients are more dispersed when evaluated on the lateral surface just downstream the separation point. It follows that the lift correlation coefficient is more dispersed than the drag one. Finally, an asymmetry of the time-averaged flow has been recognized in both preliminary wind tunnel tests and in computational simulations. This may be again explained by the extreme sensitivity of the flow to small uncontrolled uncertainties which can, in some cases, trigger the asymmetry of the mean flow.
Note that the uncertainty sources in numerical simulations are different than in experiments, but all produce similar dispersion. This confirms the difficulty in identifying a reference experiment or simulation for the considered flow configuration, while ensemble statistics over a sufficiently large number of realisations seem to be more suitable to characterize at least some of the flow properties and of the aerodynamic loads. The BARC activity is planned to continue up to 2015 under the umbrella of the International Association for Wind Engineering and in collaboration with the European Research Community On Flow, Turbulence And Combustion. In this framework, the authors hope to see the number of the flow realisations in the ensemble increased, in order to allow more precise statistics to be obtained including high-order moments and per-

centiles. In particular, collaborative studies combining wind tunnel tests and computational simulations are encouraged. The complete database of the ensemble and its statistics will be made available online from the BARC website to the interested scientific and technical communities. Such a database may allow the performance of a measurement/simulation to be put and evaluated in a probabilistic context, or the results obtained from probabilistic models, such as e.g. those used for uncertainty quantification, to be directly compared in probabilistic terms. Furthermore, the BARC test case could be ported on the ERCOFTAC QNET-CFD Knowledge Base Wiki. From a fundamental viewpoint, a deeper analysis of the averaged flow asymmetry and of its causes is encouraged. Finally, a Best Practice Advice could be developed for wind tunnel tests and computational simulations of these kind of flow.

## Acknowledgments

The authors wish to thank the Italian National Association for Wind Engineering (ANIV) for its support, the International Association for Wind Engineering (IAWE) for its promotion and the European Research Community On Flow, Turbulence And Combustion (ERCOFTAC) for its cooperation. The members of the BARC organizing committee and of the international advisory board are aknowledged for their valuable scientific supervision. In particular, special thanks go to G. Buresti for useful discussions and suggestions. The authors thank all the participants to the BARC benchmark and to the BARC special session at 13rd International Conference of Wind Engineering for the presented results and for the following stimulating debate.

## References

Arslan, T., Pettersen B., Andersson H.I., 2011. Calculations of the flow around rectangular shaped floating structures, In: Proceedings of the thirteenth International Conference on Wind Engineering, Amsterdam, The Netherlands.

Bartoli, G., Bruno, L., Buresti, G., Ricciarelli, F., Salvetti, M.V., Zasso, A., 2008a. BARC Overview Document. http://www.aniv-iawe.org/barc.

Bartoli, G., Bruno, L., Buresti, G., Ricciarelli, F., Salvetti, M.V., Zasso, A., 2008b. Requests for Computational Simulations. http://www.aniv-iawe.org/barc.

Bartoli, G., Bruno, L., Buresti, G., Ricciarelli, F., Salvetti, M.V., Zasso, A., 2008c. Requests for Wind Tunnel Tests. http://www.aniv-iawe.org/barc.

Bartoli, G., Borsani, A., Mannini, C., Marra, A.M., Procino, L., Ricciardelli, F., 2011. Wind tunnel study on the aerodynamics of a 5:1 rectangular cylin-

der in smooth flow, In: Proceedings of the thirteenth International Conference on Wind Engineering, Amsterdam, The Netherlands.

Bearman, P.W., 1969. On vortex shedding from a circular cylinder in the critical Reynolds number regime. Journal of Fluid Mechanics 37, 577-585.

Bronkhorst, A.J., Geurts, C.P.W., van Bentum, C.A., 2011. Unsteady pressure measurements on a 5:1 rectangular cylinder, In: Proceedings of the thirteenth International Conference on Wind Engineering, Amsterdam, The Netherlands.

Bruno, L., Fransos, D., Coste, N., Bosco, A., 2010. 3D flow around a rectangular cylinder: a computational study. Journal of Wind Engineering and Industrial Aerodynamics 98, 263–276.

Bruno, L., Fransos, D., 2011. Probabilistic evaluation of the aerodynamic properties of a bridge deck. Journal of Wind Engineering and Industrial Aerodynamics 99, 718–728.

Bruno, L., Coste, N., Fransos, D., 2011. Effect of the spanwise features of the computational domain on the simulated flow around a rectangular 5:1 cylinder, In: Proceedings of the thirteenth International Conference on Wind Engineering, Amsterdam, The Netherlands.

Bruno, L., Coste, N., Fransos, D., 2012. Simulated flow around a rectangular 5:1 cylinder: Spanwise discretisation effects and emerging flow features. Journal of Wind Engineering and Industrial Aerodynamics 104–106, 203–215.

Carassale, L., 2008. Flow-induced actions on cylinders in statistically-symmetric cross flow. Probabilistic Engineering Mechanics 24(3), 323–339.

De Grenet, E.T., Ricciardelli, F., 2005. The span-wise correlation of aerodynamic forces on a rectangular cylinder for different vibration regimes. In: Proceedings of the 6th European Conference on Structural Dynamics Eurodyn 2005, Paris, France.

Ercoftac test case LES2, Ercoftac database case 43.
URL http://ercoftac.mech.surrey.ac.uk/LESig/les2/homepage.html

Ercoftac QNET-CFD Knowledge Base Wiki, Underlying Flow Regime UFR2-02.
URL http://uriah.dedi.melbourne.co.uk/w/index.php/Flow_past_cylinder

Grozescu, A.N., Salvetti, M.V., Camarri, S., Buresti, G., 2011. Variational multiscale large-eddy simulations of the BARC flow configuration. In: Proceedings of the thirteenth International Conference on Wind Engineering, Amsterdam, The Netherlands.

Grozescu, A.N., Bruno, L., Fransos, D., Salvetti, M.V., 2011. Large-eddy simulations of of a Benchmark on the Aerodynamics of a Rectangular 5:1 Cylinder. In: Proceedings of the 20th Italian Conference on Theoretical and Applied Mechanics, Bologna, Italy.

Han X., Pierre Sagaut P., Lucor D., 2012. On sensitivity of RANS simulations to uncertain turbulent inflow conditions. Computers & Fluids 61, 2–5.

Hourigan, K., Thompson, M. C., Tan, B. T., 2001. Self-sustained oscillations in flows around long blunt plates. Journal Fluid and Structures 15, 387–398.

Knisely, C.W., 1990. Strouhal numbers of rectangular cylinders at incidence: a review and new data. Journal of Fluids and Structures 4(4), 371–393.

Le, T., Matsumoto, M., Shirato H., 2009. Spanwise coherent structure of wind turbulence and induced pressure on rectangular cylinders. Wind & Structures 2(5), 441–455.

Lyn, D.A., Einav, S., Rodi, W., Park, J.H., 1995. A laser-Doppler velocimetry study of ensemble-averaged characteristics of the turbulent wake of a square cylinder. Journal of Fluid Mechanics 304, 285–319.

Mannini, C., Weinman, K., Šoda, A., Schewe, G., 2009. Three-dimensional numerical simulation of flow around a 1:5 rectangular cylinder. In: Proceedings of EACWE 5, Florence, Italy.

Mannini, C., Šoda, A., Schewe, G., 2010. Unsteady RANS modelling of flow past a rectangular cylinder: Investigation of Reynolds number effects. Computational Fluids 39(9), 1609–1624.

Mannini, C., Šoda, A., Schewe, G., 2011. Numerical investigation on the three-dimensional unsteady flow past a 5:1 rectangular cylinder. Journal of Wind Engineering and Industrial Aerodynamics 99, 469–482.

Mannini, Schewe, G., 2011. Numerical study on the three-dimensional unsteady flow past a 5:1 rectangular cylinder using the DES approach, In: Proceedings of the thirteenth International Conference on Wind Engineering, Amsterdam, The Netherlands.

Matsumoto, M., Shirato, H., Aaraki, K., Haramura, T., Hashimoto, T., 2003. Spanwise coherence characteristic of surface pressure field on 2D bluff bodies. Journal of Wind Engineering and Industrial Aerodynamics 91, 155–163.

Matsumoto, M., Yagi, T., Hashimoto, M., Nakase, T., Maeta, K., Hori, K., Kawasima, Y., 2008. Steady Galloping /Unsteady Galloping and Vortex-induced Vibration of Bluff Bodies associated with Mitigation of Karman Vortex Shedding. In: Proceedings of the 6th International Colloquium on Bluff Body Aerodynamics and Applications, Milan, Italy.

McLean, I., Gartshore, I., 1992. Spanwise correlations of pressure on a rigid square section cylinder. Journal of Wind Engineering and Industrial Aerodynamics 41, 797–808.

Nakaguchi, H., Hashimoto, K., Muto, S., 1968. An experimental study on aerodynamicdrag of rectangular cylinders. Journal of the Japan Society of Aeronautical and Space Sciences 16, 1–5

Nakamura, Y., Mizota, T., 1975. Torsional flutter of rectangular prisms. Journal of the Engineering Mechanics Division 101(EM2), 125-142.

Nakamura, Y., Yoshimura, T., 1982. Flutter and vortex excitation of rectangular prisms in pure torsion in smooth and turbulentflows. Journal of Sound and Vibration 84(3), 305–317.

Nakamura, Y., Nakashima, M., 1986. Vortex excitation of prisms with elongated rectangular, H and —- cross-sections. Journal of Fluid Mechanics 163, 149–169.

Nakamura, Y., Ohya, Y., Tsuruta, H., 1991. Experiments on vortex shedding from flat plates with square leading and trailing edges. Journal of Fluid

Mechanics 222, 437–447.
Nakamura, Y., Ohya, Y., Ozono, S., Nakamaya, R., 1996. Experimental and numerical analysis of vortex shedding from elongated rectangular cylinders at low Reynolds numbers 200-1000. Journal of Wind Engineering and Industrial Aerodynamics 65, 301–308.
Namiranian, F., Gartshore, I., 1988. Direct measurements of oscillating lift on a rigid square section cylinder in a turbulent stream. Journal of Wind Engineering and Industrial Aerodynamics 28, 209–218.
Ohya, Y., Nakamura, Y., Ozono, S., Nakamaya, R., 1992. A numerical study of vortex shedding from flat plates with square lading and trailing edges. Journal of Fluid Mechanics 236, 445–460.
Oka, S., Ishihara, T., 2009. Numerical study of aerodynamic characteristics of a square prism in a uniform flow, Journal of Wind Engineering and Industrial Aerodynamics 97, 548–559.
Okajima, A., 1982. Strouhal numbers of rectangular cylinders. Journal of Fluid Mechanics 123, 379–398.
Okajima, A., Sugitani, K., Mizota, T., 1983. Strouhal Number and Base Pressure Coefficient of Rectangular Cylinders : The Case of a Section of a Width/Height Ratio of 1-9. Transactions of the Japan Society of Mechanical Engineers Series B, 49(447), 2551–2558.
Parker, R., Welsh, M.C., 1983. Effects of sound on flow separation from blunt flat plates. International Journal of Heat and Fluid Flow 4(2), 113–127.
Ribeiro, A.F.P., 2011. Unsteady RANS modelling of flow past a rectangular 5:1 cylinder: investigation of edge sharpness effects, In: Proceedings of the thirteenth International Conference on Wind Engineering, Amsterdam, The Netherlands.
Ricciardelli, F., Marra, A.M., 2008. Sectional aerodynamic forces and their longitudinal correlation on a vibrating 5:1 rectangular cylinder. In: Proceedings of the 6th International Colloquium on Bluff Body Aerodynamics and Applications, Milan, Italy.
Ricciardelli, F., 2010. Effects of the vibration regime on the spanwise correlation of the aerodynamic forces on a 5:1 rectangular cylinder, Journal of Wind Engineering and Industrial Aerodynamics 98, 215–225.
Rodi, W., 1997. Comparison of LES and RANS calculations of the flow around bluff bodies, Journal of Wind Engineering and Industrial Aerodynamics 69–71, 55–75.
Rodi, W., 2002. Large-Eddy Simulations of the Flow Past Bluff Bodies. In: Launder, B.E., Sandham, N.D. (Eds.), Closure strategies for turbulent and transitional flows. Cambridge University Press, 361-391.
Schewe, G., 1983. On the Force Fluctuations Acting on a Circular Cylinder in Cross Flow From Subcritical up to Transcritical Reynolds Numbers, Journal of Fluid Mechanics 153, 265–285.
Schewe, G., 2006. Influence of the Reynolds-number on flow-induced vibrations of generic bridge sections. In:Radič J. (Ed.), Proceedings of the International Conference on Bridges, Dubrovnik, Croatia, 351358.

Schewe, G., 2009. Reynolds-number-effects in flow around a rectangular cylinder with aspectratio1:5. In: Proceedings of the Fifth European and African Conference on Wind Engineering, Florence, Italy.

Shimada, K. Ishihara, T., 2002. Application of a modified $k - \varepsilon$ model to the prediction of aerodynamic characteristics of rectangular cross-section cylinders. Journal of Fluids and Structures 16 (4), 465-485.

Shirato, H., Yuichi, S., Sasaki, O., Van Baod, D., 2010. Coherent structure of surface pressures on 2-D rectangular cylinders, In: Proceedings of the fifth International Symposium on Computational Wind Engineering, Chapel Hill, North Carolina, USA.

Shirato, H., Yuichi, S., Sasaki, O., 2011. Surface pressure correlation and buffeting force evaluation, In: Proceedings of the thirteenth International Conference on Wind Engineering, Amsterdam, The Netherlands.

Spalart, P.R. and Allmaras, S.R., 1992. A one-equation turbulence model for aerodynamic flows. Proceedings of 30th AIAA Aerospace Sciences Meeting and Exhibit, Reno (NV), USA, 92.

Spalart, P.R., Jou, W.-H., Stretlets, M. and Allmaras, S.R, 1997. Comments on the Feasibility of LES for Wings and on the Hybrid RANS/LES Approach. Proceedings of the First AFOSR International Conference on DNS/LES, Ruston, Louisiana, USA.

Stokes, A.N., Welsh, M.C., 1986. Flow-resonant sound interaction in a duct containing a plate, II:square leading edge. Journal of Sound and Vibration 104(1), 55-73.

Tamura, T., Ito, Y., Kuwahara, K., 1993. Computational separated-reattaching flows around a rectangular cylinder, Journal of Wind Engineering and Industrial Aerodynamics 50, 9–18.

Tamura, T., Ito, Y., Wada, A., Kuwahara, K., 1995. Numerical study of pressure fluctuations on a rectangular cylinder in aerodynamic oscillations, Journal of Wind Engineering and Industrial Aerodynamics 54/55, 239–250.

Tamura, T., Ito, Y., 1996. Aerodynamic characteristics and flow structures around a rectangular cylinder with a section of various depth/breadth ratios. Journal of Structural and Construction Engineering 486, 153-162 (in Japanese).

Tamura, T., Miyagi, T., Kitagishi, T., 1998. Numerical prediction of unsteady pressures on a square cylinder with various corner shapes. Journal of Wind Engineering and Industrial Aerodynamics 74-76, 531–542.

Tan, B.T., Thompson, M.C., Hourigan, F., 2004. Flow past rectangular cylinders: receptivity to transverse forcing. Journal of Fluid Mechanics 515, 33–62.

Travin, A.K., Shur, M.L., Strelets, M.Kh., Spalart, P.R., 1999. Detached-eddysimulations past a circular cylinder. Flow Turbulence and Combustion 63(14), 293–313.

Vickery, B.J., 1996. Fluctuating lift and drag on a long cylinder of square cross-section in a smooth and in a turbulent stream. Journal of Fluid Mechanics 25, 481–494.

Voke, P.R., 1997. Flow past a square cylinder: test LES2, In: Direct and Large-Eddy Simulation II, J.P. Chollet et al. (eds.), ERCOFTAC Series, vol. 5, Kluwer Academic Publishers, 355–373.

Yu, D., Kareem, A., 1998. Parametric study of flow around rectangular prisms using LES. Journal of Wind Engineering and Industrial Aerodynamics 77-78, 653–662.

Wei, Z., Kareem, A., 2011. A benchmark study of flow around a rectangular cylinder with aspect ratio 1:5 at Reynolds number 1.E5, In: Proceedings of the thirteenth International Conference on Wind Engineering, Amsterdam, The Netherlands.